Heritage Science

RESEARCH

Open Access

The spectral inversion model for electrical conductivity in mural plaster following phosphate erosion based on fractional order differentiation and novel spectral indices

Yikang Ren[1,2] and Fang Liu[1,2*]

Abstract

The Dunhuang murals are a precious treasure of China's cultural heritage, yet they have long been affected by salt damage. Traditional methods for detecting salt content are costly, inefficient, and may cause physical harm to the murals. Among current techniques for measuring salt content in murals, hyperspectral remote sensing technology offers a non-invasive, circumventing issues of high costs, low efficiency. Building on this, the study constructs an inversion model for the Electrical Conductivity (EC) values of mural plaster subjected to phosphate erosion, through the integration of Fractional Order Differentiation (FOD), a novel three-band spectral index, and the Partial Least Squares Regression algorithm. The specific research contents include: (1) Initially, in preparation for the experiments, the materials used to create the samples underwent a rigorous desalting process, and phosphate solutions were prepared using deionized water to ensure uniform experimental conditions and the accuracy of the results. These meticulous preprocessing steps guaranteed that the measured EC values exhibited a clear correlation with the phosphate content. Subsequently, by employing qualitative experimental analysis techniques, this study was able to more accurately simulate the real-world scenarios of mural plaster affected by salt damage, enabling a deeper investigation into the mechanisms by which salts inflict microscopic damage to murals. (2) Explores the absorption mechanisms and characteristic spectral bands of the Electrical Conductivity (EC) values measured after the phosphate erosion of mural plaster. By integrating the optimal spectral indices, a univariate linear regression model is constructed, providing a basis for the rapid quantitative measurement of electrical conductivity in murals. (3) By comparing the accuracy of the Phosphate Simple Ratio (PSR) and Phosphate Normalized Difference Index (PNDI) spectral indices based on the linear regression model, the first six orders of the highest accuracy spectral index were selected as the optimal three-band spectral index combination, used as explanatory variables, with mural plaster electrical conductivity as the response variable, employing the PLSR method to construct the mural phosphate content high-spectral feature inversion model. The study's findings include: (1) Surfaces of samples deteriorated by phosphate erosion formed numerous irregularly shaped crystal clusters, exhibiting uneven characteristics. (2) By comparing the outcomes of different orders of fractional differentiation, it was found that the model performance reached its optimum at a 0.3 order of differentiation for both PSR and PNDI data, with a determination coefficient (Q^2) of 0.728. (3)

*Correspondence:
Fang Liu
lf@bucea.edu.cn
Full list of author information is available at the end of the article

Utilizing PLSR, this study employed the previously determined optimal six-order three-band spectral index combination as explanatory variables, with salt content as the response variable, successfully constructing the high-spectral feature inversion model for mural electrical conductivity with a determination coefficient (Q^2) of 0.815. This provides an effective technical means for monitoring the salt damage conditions of precious cultural heritage such as murals.

Keywords Mural salt damage, Fractional order differential preprocessing, Correlation coefficient, Partial least squares regression, Spectral index

Introduction

Ancient mural sites, serving as a vivid annotation of history, not only chronicle the evolution of human civilization but also mirror the levels of production and daily life in ancient societies. In China, the Dunhuang murals, heralded as national treasures of cultural heritage, are world-renowned for their rich themes, exquisite craftsmanship, and unique historical significance. These murals not only depict the religious beliefs, social life, and artistic styles from over a millennium ago but also constitute invaluable resources for the study of cultural exchanges along the ancient Silk Road [1–5]. Regrettably, due to the ravages of time and environmental influences, these murals have suffered from various forms of degradation, including fading, efflorescence, erosion by windblown sand, and mold growth. The detachment of the pigment layer from the mural plaster underlay, as well as the separation of the plaster layer from the cliff's supporting strata, has gravely compromised the aesthetic appeal and historical value of these artworks [6, 7].

At present, the quantitative detection of salt content in murals primarily involves sample analysis. Suzhen Yan and her team the Merckoquant qualitative test strip method to conduct a survey and analysis of salt damage in Cave 276 [8]. Du Hongying and her team used Capillary Electrophoresis (CE), also known as High Performance Capillary Electrophoresis (HPCE), to investigate the occurrence and development patterns of salt damage in murals by defining the relationships between characteristic system temperatures, in conjunction with the actual environment of the Mogao Grottoes. This method allows for a scientific elucidation of the intrinsic process mechanisms behind various surface phenomena of salt-damaged murals, and analyzes the critical values of safe salt content in murals and environmental conditions [9]. Yuzong Ren and associates chose the severely damaged areas of the Buddha platform and fan-shaped wall murals in the Longxing Temple's Mani Hall as their research subjects, utilizing ion chromatography to analyze soluble salts [10]. However, the methodologies employed by the aforementioned researchers all require physical sampling, which inevitably inflicts a certain degree of damage on the murals. In the study of mural salt content, hyperspectral remote sensing technology offers valuable information about the chemical composition, spatial distribution, content estimation, crystallization monitoring, environmental impact, and non-destructive testing [11–15]. It reveals the aforementioned characteristics through the forms of spectral reflection and absorption. Concurrently, hyperspectral remote sensing technology, as a non-contact and non-destructive method, has demonstrated significant potential in the domain of cultural heritage conservation [16]. By analyzing the spectral data reflected from the surface of murals, hyperspectral technology is capable of precisely identifying and quantifying the types and distribution of salts within the murals. This approach not only effectively circumvents the potential physical damage to cultural heritage that may arise from traditional sampling analysis but also provides more comprehensive and detailed data on salt damage. Consequently, it furnishes a more scientific basis for the conservation and restoration of murals. Furthermore, the application of hyperspectral technology facilitates the monitoring of subtle changes in the mural environment, predicts potential salt damage risks, and assesses the efficacy of conservation measures, thereby offering an advanced and effective technological means for the long-term protection of cultural heritage [17]. Through this modality, researchers and conservation experts can more accurately understand and manage the impact of salt damage on murals, ensuring that these irreplaceable cultural assets are better protected.

Furthermore, although the impact of phosphates in murals has not been as extensively studied as that of chlorides or sulfates, their potential influence on cultural heritage still receives considerable attention. Literature on the conservation of cultural heritage, such as the Dunhuang murals [18, 19], suggests that the effects of phosphates are often associated with microbial activity, materials used in historical restorations, or environmental factors (such as temperature, humidity, and rainfall), all of which can contribute to the accumulation of phosphates. By monitoring the variations in phosphate levels within murals, researchers can gain a deeper understanding of how environmental conditions influence the conservation status of these artworks. Moreover, the degradation of the porous substrate layers in ancient murals is primarily caused by two factors: first, the chemical

erosion from salt solutions within the material, and second, the cumulative effect of temperature and humidity fluctuations causing repeated cycles of crystallization and dissolution. The latter is the predominant factor leading to the expansion and fracturing of the substrate layer's pores. Given that phosphates can form dodecahydrate under specific hydrothermal conditions, this could lead to repeated cycles of crystallization and dissolution [20]. The physical properties of phosphates make them one of the salts that pose a threat to cultural heritage, hence understanding this process is crucial for developing effective conservation measures. Through hyperspectral remote sensing technology, we can detect and analyze these salts in a non-invasive manner, offering new methodologies for preventing and mitigating salt damage.

Consequently, this study concentrates on inverting the Electrical Conductivity (EC) values of mural plaster subjected to phosphate erosion using a novel three-band salinity spectral index. The aim is to develop a more precise inversion model through the analysis of spectral data from desalinated mural plaster samples. Current research on salt content in mural plaster largely relies on traditional integral order differentiation and salt spectral indices to construct inversion models. The application of fractional order differentiation in this field is scarcely understood, particularly regarding the investigation of phosphate content in mural plaster, where existing literature is limited and lacks precise inversion studies on different physical states of phosphate content. Given that phosphates can form dodecahydrate under certain hydrothermal conditions, this physical property positions them as one of the primary salts posing threats to cultural heritage, presenting higher challenges for the preservation of cultural artifacts compared to common sulfates [21]. In light of this backdrop, our research endeavors to enhance the accuracy of electrical conductivity inversion in mural plaster by establishing a new three-band salt index, thereby striving to address the gaps in current studies within this domain. Simultaneously, this study aims to provide new perspectives and references for future precise inversion issues regarding different physical states of phosphates.

Although the application of hyperspectral remote sensing technology in predicting soil salinity content demonstrates vast potential, achieving high accuracy currently faces several challenges and discrepancies [22–24]. To enhance the sensitivity of spectral bands, mathematical differential transformations are extensively employed in the realm of hyperspectral data mining [25, 26]. Integer order differentiation is a common method for preprocessing hyperspectral data, with numerous studies having utilized first and second order differentiation to identify salt-sensitive wavelength bands for mural paintings and to construct their inversion models, demonstrating certain potential for application [17]. However, it has also been observed that integer order differentiation (e.g., first and second order) can introduce noise and compromise some useful information, thereby affecting the performance of estimation models [27]. In contrast, fractional order differentiation offers a more flexible framework, capable of capturing finer spectral variations, especially exhibiting superior performance in handling nonlinear and complex physical processes. Recent advancements in fractional order differentiation techniques and their application suggest that, with the development of computational technology and data processing algorithms, an increasing number of studies are exploring the application of fractional order differentiation in spectral analysis, particularly in the quantitative remote sensing research of soil, vegetation, and other surface characteristics [28]. For instance, Zhang et al. collected soil from the northwest region of China, measured indoor hyperspectral data, analyzed organic matter content, and conducted fractional order derivative (FOD) preprocessing of soil hyperspectral data at intervals of 0.05 [29]. Simulation results indicated that within the magnitude range of 1.05–1.45, the correlation between FOD and organic matter was optimal. Xiangyu Ge and others proposed a framework with lower uncertainty for estimating soil salinity using GF-5 hyperspectral data, which can be utilized for estimating soil salinity. FOD technology can enhance the correlation between soil salinity and spectra, identify diagnostic characteristic bands, and reduce the model's uncertainty [30]. Although fractional order differentiation theoretically holds advantages, how to select the most appropriate order of differentiation, address uncertainties and complexities in the computation process, and integrate these methods with existing remote sensing data processing workflows remain areas that require further research and exploration.

The utilization of spectral indices constitutes a straightforward and efficacious methodology for measuring surface properties, with band optimization algorithms extensively applied in the development of hyperspectral technology [29]. Compared to one-dimensional spectral data, this approach affords a richer spectrum of spectral features, thereby fortifying the correlation between soil properties and spectral characteristics [31]. For instance, research conducted by Chen et al. [32] delves into the efficacy of visible-near infrared spectroscopy in estimating the content of heavy metals in soil. Through an analysis of 120 soil samples collected in Xuzhou City, Jiangsu Province, not only were the heavy metal content and spectral characteristics of the samples determined, but attempts were also made to enhance the spectral information of soil heavy metals through fractional order

derivative spectral preprocessing methods (FOD) and a novel three-band index, concurrently addressing issues of collinearity and redundancy inherent in hyperspectral data. Yuan et al. [33] proposed a soil organic matter content estimation method based on an improved Hapke model, anchored in the radiative transfer process of soil reflectance spectra. By transforming reflectance and single scattering albedo, they constructed spectral indices, thus facilitating the remote sensing estimation of soil organic matter content. According to the aforementioned analyses, spectral indices are capable of effectively capturing the hyperspectral response of soil components, and by expressing them within two-dimensional or multidimensional spectral spaces, they mitigate interference from other soil components in estimation outcomes. Moreover, spectral indices enhance the subtle correlations between bands, simplify model structures, and eliminate redundant information variables. Therefore, applying spectral indices to quantitatively analyze the interactions between characteristic bands of phosphates in mural plaster can significantly enhance the accuracy of phosphate content estimation models. Existing research employing various spectral index combination methods (such as normalization, difference, and ratio) has leveraged hyperspectral data to explore the relationship between soil reflectance and soil components [29, 34]. Compared to dual-band spectral indices, three-band indices incorporate a third band within specific sensitive areas, a processing method that often improves the precision of the estimate, enhances interference resistance, eliminates the saturation phenomenon common to dual-band indices, rendering the estimation of soil components more robust and accurate [32, 35].

In the process of safeguarding these irreplaceable cultural assets, understanding the phosphate content within mural plaster is crucial for the prevention and treatment of salt damage. Phosphates, under certain hydrothermal conditions, can form dodecahydrates, posing a greater threat to mural cultural heritage compared to common sulfates. Therefore, this study is dedicated to simulating the capillary salt ion adsorption and crystalline erosion degradation processes within the in-situ environment of murals, a method that diverges from traditional laboratory practices of preparing samples with predetermined salt content. This approach more closely mirrors the actual conditions under which murals suffer salt damage, enabling a thorough exploration of the specific impact mechanisms of salts at the microscopic level, thereby providing a more precise and practical scientific basis for mural conservation. Simultaneously, within the design of this experiment, the extent of salt damage to samples may vary even under identical experimental conditions. This variation could be attributed to factors such as the placement angle of the samples and their contact area. Therefore, to ensure a high correlation between the measured Electrical Conductivity (EC) values and phosphate content, all materials used in sample preparation undergo rigorous desalination and are treated with phosphate solutions prepared from deionized water prior to experimentation, thus securing the accuracy of the experimental results. The incorporation of this processing step ensures that the EC values measured post-experiment exhibit a high correlation with phosphate content. Further, this study concentrates on inverting the Electrical Conductivity (EC) values of mural plaster subjected to phosphate erosion using a novel three-band salinity spectral index. The aim is to develop a more precise inversion model through the analysis of hyperspectral data from desalinated mural plaster samples. This represents a relatively novel endeavor in the field of hyperspectral remote sensing technology, where fractional order differentiation methods offer a more flexible framework capable of capturing finer spectral variations, particularly suited for handling nonlinear and complex physical processes. Additionally, the construction of a three-band spectral index as a processing method can often enhance the precision of estimates, improve interference resistance, and eliminate the saturation phenomenon common with dual-band indices. Through this method, we aim to precisely identify and quantify the types and distribution of salts within murals without inflicting physical damage, thereby providing a more scientific basis for the protection and restoration of murals. Figure 1 illustrates the migration and phase transformation mechanisms of hydrothermal salts in porous medium materials under the in-situ environment of murals.

Materials and methods

Experimental area and sample fabrication

Ancient murals were selected for study due to their distinguished historical value and the characteristic phenomena of salt damage they exhibit. The research site is located at the Mogao Caves in Dunhuang City (approximately 25 km southeast of Dunhuang City, with coordinates at 94.662° E longitude and 40.142° N latitude). Figure 2 illustrates typical types of salt damage to the murals in the research area [36], including: (a) Plaster Detachment: partial separation of the plaster layer from the supporting structure, with the detached portion still connected to the support around its periphery. This includes instances where the upper layer of double-layered murals partially detaches from the lower layer. (b) Cracks: misalignment and cracking phenomena in the murals. (c) Craquelure: fine network of surface cracking on the mural. (d) Plaster Disruption: a state of looseness

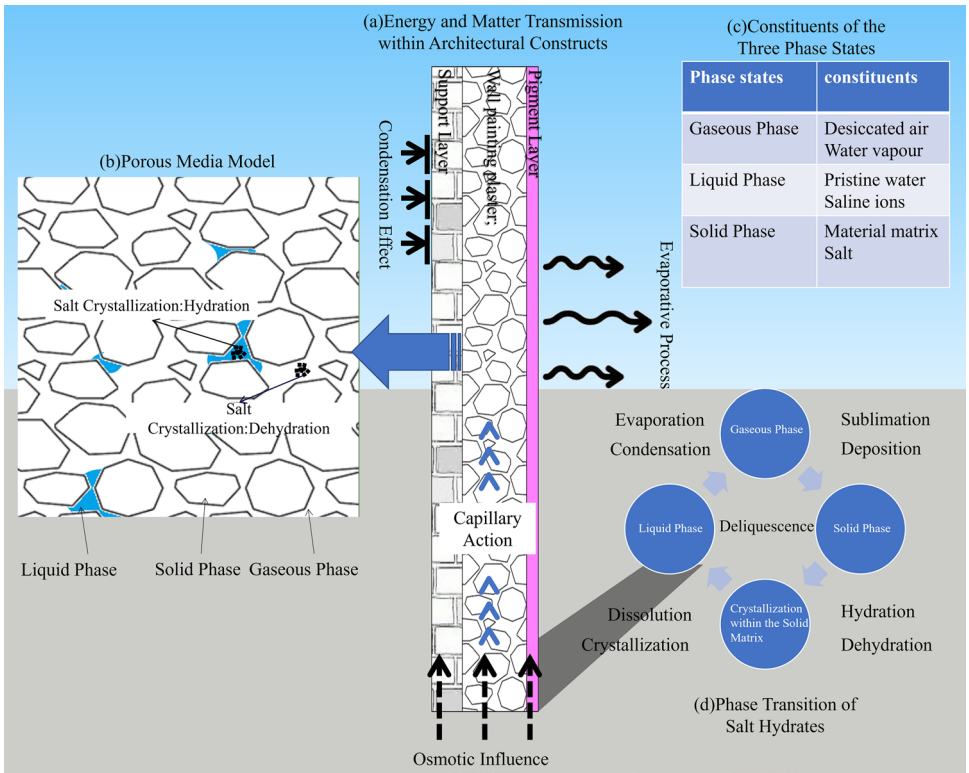

Fig. 1 Hydrothermal salt transport, porous medium model, and phase transition mechanism in the in situ environment of murals

in the mural plaster layer caused by the action of soluble salts.

The methodology for sample preparation was informed by the study conducted by Bi [37], while the desalination process adheres to the GB/T50123-2019 standard. Frist, the raw materials—kaolinite clay, sand, and wheat straw—undergo a desalination process to eliminate potential interference from salts present in the original materials on the experimental outcomes. The procedure entails sieving a certain amount of dried soil sample through a 0.56 mm sieve, mixing it with deionized water in a 1:5 ratio, and stirring clockwise for 0.5 h to dissolve the salts. Subsequently, the mixture is allowed to settle for 24 h. After the supernatant water clears, it is removed, and this desalination process is repeated a total of five times. The effectiveness of the desalination is assessed by measuring the electrical conductivity of the soil sample, ensuring the total salt content does not exceed 0.1%. Following desalination, the soil sample is dried, crushed, and sieved for later use. Then, kaolinite clay, sand, and wheat straw are mixed in a 64:36:3 ratio, and distilled water equal to 20% of the solid mass is added. The uniformly mixed materials are filled into pre-greased molds, with the surface smoothed and excess air removed by vibration. Finally, the molds are placed in an oven at 90 °C to dry, reducing the moisture content of the samples as much as possible to closely approximate a completely dry state. This series of preparatory steps is designed to fabricate mural plaster samples that meet experimental requirements, facilitating subsequent studies on the effects of salt damage.

Qualitative experimental analysis

This experiment simulates the capillary salt ion adsorption and crystallization erosion degradation process in the in-situ environment of murals, diverging from traditional laboratory methods that use samples pre-fabricated with specific salt content. This approach more closely mirrors the real-world conditions under which murals suffer from salt damage, enabling an in-depth exploration of the specific mechanisms through which salinity impacts murals at a microscopic level, thus providing a more accurate and practical scientific basis for the conservation of murals. The use of a field emission scanning electron microscope (FESEM) allows for qualitative analysis of both the original samples and those subjected to phosphate erosion, offering a better understanding of the microscopic morphology of the mural plaster layer materials. It facilitates discussions on how salts, through various physical processes and chemical reactions, cause multiple forms of degradation to murals. These diverse types of degradation phenomena

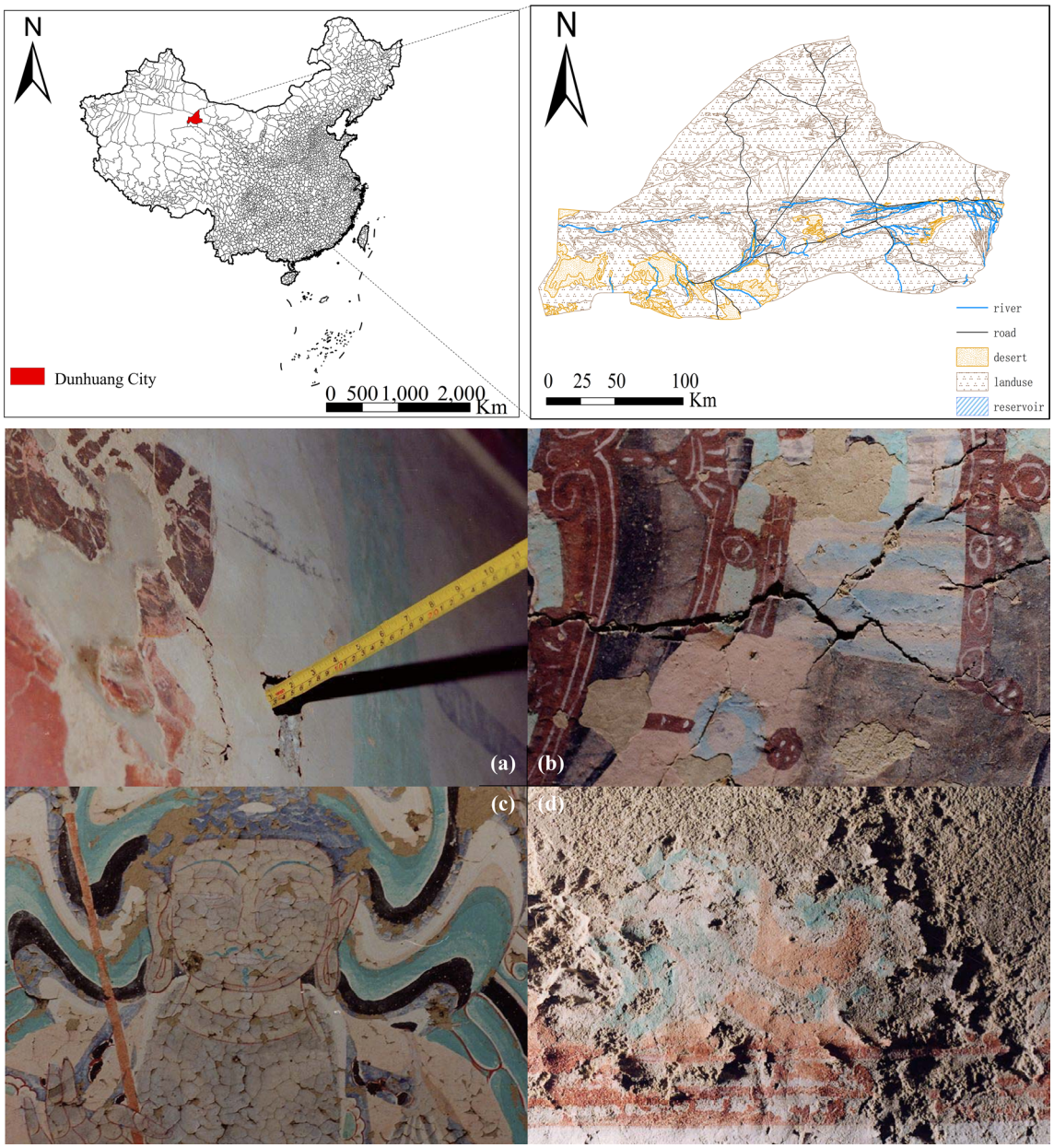

Fig. 2 Typical salt damage types in the murals of the study area. **a** Plaster detachment: partial separation of the plaster layer from the supporting structure, with the detached portion still connected to the support around its periphery. This includes instances where the upper layer of double-layered murals partially detaches from the lower layer. **b** Cracks: misalignment and cracking phenomena in the murals. **c** Craquelure: fine network of surface cracking on the mural. **d** Plaster disruption: a state of looseness in the mural plaster layer caused by the action of soluble salts

unveil the complex challenges of salt damage to mural conservation, highlighting the importance of detailed salt analysis to better understand and mitigate these effects. This experimental inquiry employs the Quanta 250 FEG field emission scanning electron microscope for subsequent discussions, with a magnification range from 15 to 300,000 times.

Data collection

To investigate the hyperspectral characteristics of Mural Plaster in response to phosphate concentrations, this experiment was designed with five different concentrations of disodium hydrogen phosphate dodecahydrate solutions: 0.608, 0.808, 1.008, 1.208, and 1.408 mol/L, representing the range from lowest to highest erosion

conditions. The samples were temperature-controlled using a high-precision, low-temperature constant temperature bath set at 32.5 °C to simulate capillary absorption effects eroding the Mural Plaster samples (a total of 100 samples, with 20 samples under each condition). This experimental methodology more accurately reflects the real-life scenario of murals affected by salt damage under natural conditions. Due to the impact of salt damage, significant changes occur in the surface and internal structure of the Mural Plaster, where variations in porosity and surface roughness are directly related to the extent of salt damage, significantly influencing the collection and analysis of spectral data [38]. Through this method, we can more effectively simulate data collection in actual environmental conditions, thereby enhancing the validity and accuracy of the model. Seventy samples were used to develop new spectral indices and phosphate inversion models, while 30 samples served as an independent testing set to evaluate our spectral indices and models. After the samples air-dried, their spectral reflectance was measured using an ASD-FieldSpec4 HI-RES spectroradiometer, collecting hyperspectral data with a wavelength range from 350 to 2500 nm and sampling intervals of 1.4 nm (350–1000 nm) and 2 nm (1001–2500 nm). To avoid interference from other light sources, measurements were conducted indoors under enclosed conditions without other light sources at night. After a 30-min instrument warm-up, standard reflectance calibration was performed. The instrument's 57 fiber optics were embedded in the ASDPanalytical (Model: A122317) high-brightness contact probe light source, a 70W quartz–tungsten–halogen lamp with a 25 mm aperture. The aperture was inverted vertically over the sample's central surface, the light source was switched on, and once the curve stabilized, data were collected. The probe was then rotated 90° parallel to the sample surface for repeated measurements, assessing four directions and then measuring the sample's center point once more, averaging these values as the sample spectral data, all completed in a dark room.

In this experiment, to eliminate potential interferences from salts in the raw materials, the raw materials underwent a desalting process. This step ensures that conductivity measurements accurately reflect changes caused by phosphates, not other salts. Conductivity measurement is a crucial indicator for assessing phosphate content in soil samples. Based on this, we hypothesized that changes in phosphate content in the samples would closely correlate with changes in conductivity, a point supported in the literature. Specifically, Zhang [39] and Ge et al. [30] indicated in their studies that the conductivity of soil solutions can effectively reflect the total salt content in the soil. Although these studies did not directly link phosphate content to conductivity, they provide compelling evidence that conductivity can indicate the salt content in the soil, thus supporting our hypothesis.

The phosphate content in the eroded mural samples was assessed by changes in electrical conductivity, with specific steps to measure conductivity as follows: In the laboratory, the mural samples post-phosphate erosion were sieved through a 2 mm soil sieve. A soil leachate was prepared at a 1:5 soil-to-water ratio and filtered at an indoor temperature of 25 °C. The soil leachate's electrical conductivity (EC) was measured using a soil salinity EC conductivity meter [30]. Figure 3 presents the flowchart for sample preparation and the collection process of hyperspectral data for mural plaster.

Statistical analysis and visualization methods for electrical conductivity data of mural plaster

For the electrical conductivity data of mural plaster under five different conditions, a statistical description was conducted, encompassing data density distribution, mean, standard deviation, minimum values, quartiles (first and third), and the coefficient of variation (CV). The coefficient of variation (CV) serves as a standardized measure of dispersion, calculated as the ratio of the standard deviation to the mean, and is utilized to assess the variability of the data. The criteria for evaluating data variability are as follows: a $CV \leq 15\%$ indicates low variability, $15\% < CV \leq 35\%$ signifies moderate variability, and a $CV > 35\%$ denotes high variability. In the graphical representations, red dashed lines depict the first and third quartiles, while blue dashed lines illustrate the mean. The formula for calculating the coefficient of variation (CV) is presented as Eq. 1:

$$CV = \frac{\sigma}{u} \times 100\%, \tag{1}$$

where CV denotes the Coefficient of Variation (expressed as a percentage), symbolized by σ, which represents the standard deviation of the sample (measured in ms m^{-1}). The symbol u corresponds to the mean value of the sample (measured in ms m^{-1}).

Spectral data preprocessing

To mitigate the impact of noise on the analysis of spectral data, the collected spectral reflectance data of mural plaster underwent preprocessing to eliminate high-frequency noise and outliers. This step involved removing the wavebands with low signal-to-noise ratios at 350–400 nm and 2401–2500 nm, and applying a smoothing process via

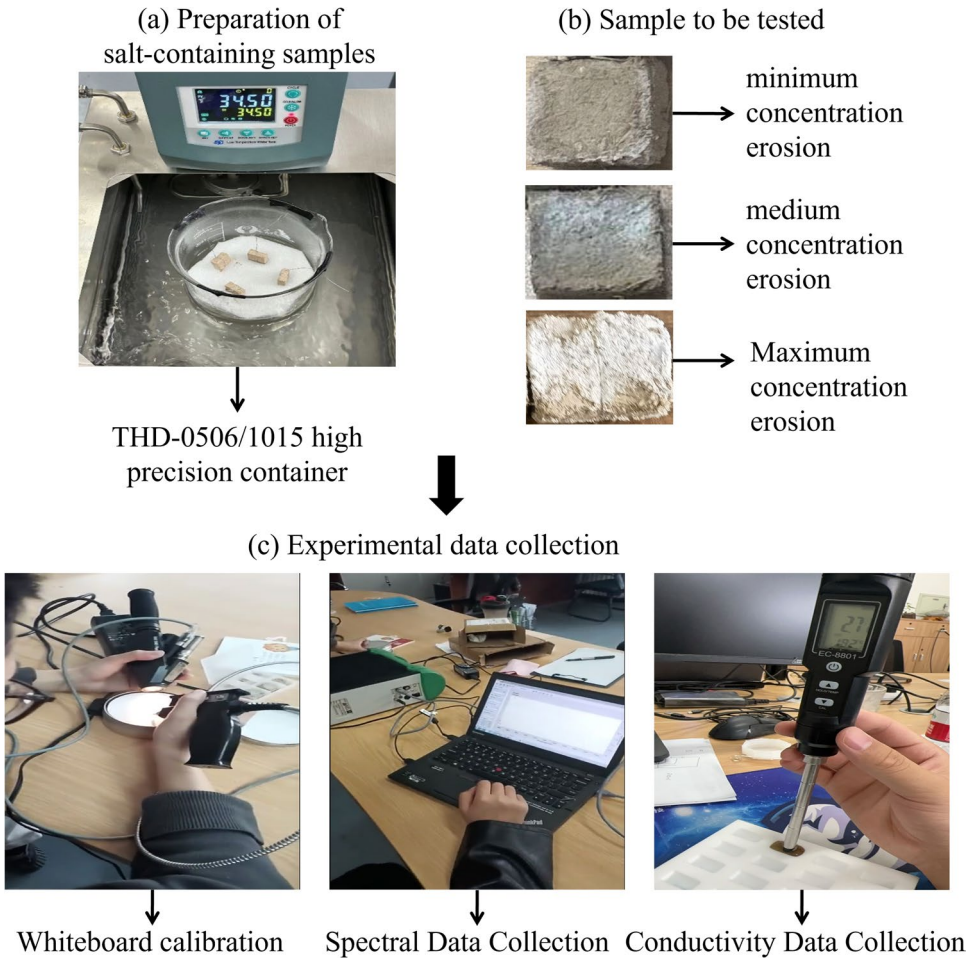

Fig. 3 Sample preparation and hyperspectral data acquisition for mural plaster

the Savitzky–Golay filter (Eq. 2) [40], utilizing a 21-point window and a second-order polynomial.

$$y_i' = \frac{1}{\Delta} \sum_{j=-m}^{m} c_j \cdot y_{i+j}, \tag{2}$$

where y_i' represents the smoothed spectral reflectance at position i, with y_{i+j} indicating the points in the original data series, and c_j denoting the coefficients in the convolution kernel. These coefficients are ascertained through polynomial fitting. The variable m is half the size of the window, Δ typically 1, unless the intervals between data points are non-uniform.

Research methods

Fractional-order derivative

Fractional Order Differential (FOD) represents an extension of traditional integer-order differentiation and manifests in various forms within the realms of mathematics and engineering [41], such as Riemann–Liouville (R–L), Lévy, Weyl, Caputo, and Grünwald–Letnikov (G–L) [42]. The Grünwald–Letnikov method, owing to its suitability for handling discrete data, has found extensive application in engineering and scientific fields. A primary advantage of this method lies in its direct foundation upon the difference definition of differentiation, which facilitates its application in numerical computations to be more straightforward and convenient. Particularly in dealing with discrete data such as hyperspectral signals, the Grünwald–Letnikov method demonstrates its unique applicability [28]. Consequently, pursuant to the Grünwald-Letnikov algorithm, the fractional order (v) of f(x) within the wavelength domain [a, t] can be delineated as depicted in Eq. (3). Γ denotes the Gamma function ($\Gamma(v) = (v-1)!$).

$$\mathrm{d}^{\mathrm{v}}\mathrm{f}(\mathrm{x}) = \lim_{h \to 0} \frac{1}{\mathrm{h}^{\mathrm{v}}} \sum_{n=0}^{[(t-a)/h]} (-1)^{\mathrm{n}} \frac{\Gamma(v+1)}{\mathrm{n}!\Gamma(v-n+1)} \mathrm{f}(\mathrm{x}-n\mathrm{h}), \tag{3}$$

where v is the fractional order, h is the step size, t and a is the upper and lower bounds of fractional order differentiation.

In this experiment, assuming the function f (x) as a one-dimensional hyperspectral signal with a band range of [a, t], where x∈[a, t] divided by the differential step length h. Given that the ASD FieldSpec® 4 Hi-Res Spectrometer's retention interval is 1 nm, the differential step length can be set to h = 1. Consequently, the expression for the v-th order fractional differentiation of the function f (x) can be derived from Eq. (3) as follows:

$$\begin{aligned}\frac{d^{v}f(x)}{dx^{v}} \approx & f(x)+(-v)f(x-1)+\frac{(-v)(-v+1)}{2}f(x-2)\\ & +\frac{(-v)(-v+1)(-v+2)}{6}f(x-3)+\\ & \cdots+\frac{\Gamma(-v+1)}{n!\Gamma(-v+n+1)}f(x-n),\end{aligned} \tag{4}$$

where v is the fractional order, x is the wavelength.

Construction of the spectral reflectance index

In recent years, numerous studies have focused on estimating soil components through spectral indices, particularly by employing dual-band spectral indices [43, 44]. These indices facilitate the elucidation of both the external responses and intrinsic meanings of spectral data, and they are capable of amplifying the subtle correlations between bands. Concurrently, the Phosphate Simple Ratio (PSR) and the Phosphate Normalized Difference Index (PNDI) place the strongest and weakest reflection bands in the numerator and denominator, respectively. Through operations of ratios and normalized ratios, they further expand the disparity between bands to maximize the sensitivity of the measured property attributes [45]. The constructions of the PSR index and the PNDI index are represented by Eqs. 5 and 6, respectively.

$$PSR=\frac{R_a}{R_b}, \tag{5}$$

$$PNDI=\frac{R_a-R_b}{R_a+R_b}, \tag{6}$$

where R_a and R_b each denote the spectral reflectance at a given wavelength.

In this study, we introduce a novel three-band index—Phosphate Three Simple Ratio (PTSR)—aimed at enhancing the precision of spectral index estimates and bolstering their resistance to interference, thereby improving the monitoring of electrical conductivity in mural plaster. The design process of this spectral index encompasses several steps, beginning with the selection of spectral indices most closely correlated with electrical conductivity in mural plaster, as determined by calculating the correlation coefficients between electrical conductivity and both the PSR and PNDI spectral indices. This involves conducting univariate regression analysis on the spectral indices with the highest correlation coefficients at each order, to identify the optimal spectral indices for each tier.

Further, by analyzing the best-performing spectral indices from the univariate regressions up to the sixth order, these indices were utilized as explanatory variables in a Partial Least Squares Regression (PLSR) analysis of ground electrical conductivity. In the accuracy comparison between the PSR–PLSR and PNDI–PLSR models, the best-performing model was selected as the basis for the three-band index study. Rc, denoting the waveband corresponding to the spectral index with the highest correlation coefficient with electrical conductivity, was incorporated as a specific sensitive waveband to further refine the spectral index design. The ultimately formulated three-band index, PTSR, is defined as Eq. 7:

$$PTSR=\frac{R_a}{R_b-R_c}, \tag{7}$$

where R_a and R_b represent the reflectance at specific wavebands a and b within the range of 400–2400 nm, respectively, while R_c denotes a particular waveband selected based on the optimal model.

Correlation coefficient

In the realm of statistics, the Pearson correlation coefficient is a widely employed method for analyzing the relationships between variables. It quantifies the strength of association between two vectors based on their covariance matrix. The formula for calculating the Pearson correlation coefficient is denoted as Eq. 8 [46]:

$$P(\alpha_i,\alpha_j)=\frac{\operatorname{cov}(\alpha_i,\alpha_j)}{\sqrt{\operatorname{var}(\alpha_i)\times\operatorname{var}(\alpha_j)}} \tag{8}$$

where $\operatorname{cov}(\alpha_i,\alpha_j)$ represents the covariance, $\operatorname{var}(\alpha_i)$ denotes the variance of α_i, $\operatorname{var}(\alpha_j)$ denotes the variance of α_j.

Modeling process for mural plaster electrical conductivity using fractional order differentiation and three-band index-based partial least squares regression

In this study, univariate regression and Partial Least Squares (PLS) regression are employed to estimate the

electrical conductivity in mural plaster [47]. Univariate regression refers to a method involving only one independent variable and one dependent variable. For variable selection, the Pearson correlation coefficient is used to measure the strength of the linear relationship between the independent and dependent variables. This paper calculates the correlation coefficients between the PNDI, PSR, PTSR spectral indices, and the electrical conductivity in mural plaster. The absolute value of the correlation coefficient describes the degree of linear correlation between two variables [48]. Consequently, this research selects the spectral index corresponding to the highest correlation coefficient as the independent variable, with the electrical conductivity in mural plaster as the dependent variable. The test and validation sets are split in a 7:3 ratio, conducting univariate regression to identify the optimal order and band position, providing a basis for establishing a multivariate regression model subsequently.

In this research, the objective is to develop an inversion model to analyze the electrical conductivity (EC) of mural plaster and its variations under different concentrations of erosion conditions. The spectral indices derived from the optimal orders up to the sixth order, identified through PNDI and PSR screening, serve as explanatory variables, and the corresponding electrical conductivity of mural plaster (response variable) is utilized to establish a Partial Least Squares Regression (PLSR) model. The accuracy of the PNDI–PLSR model and the PSR–PLSR model is compared to determine the foundational indices for constructing a novel three-band index. Finally, Eqs. 4 and 7 are used to establish a PLSR model for mural plaster phosphate based on Fractional Order Differentiation (FOD) and the three-band index (explanatory variable), with the corresponding electrical conductivity of mural plaster (response variable).

To enhance the model's precision, data underwent standardization and mean centering as preprocessing steps. The model's framework is based on the Kernel PLS algorithm, with the number of principal components capped at seven. Optimal component numbers were determined through random cross-validation, and specific model warning parameters were set (thresholds for the calibration and validation residual variance ratio set at 0.5 and 0.75, respectively, and the upper limit for residual variance increase set at 6%) to ensure the model's stability and reliability.

In this study, the selection of specific three-band bands no longer simply relies on the outcomes of previous research but instead employs a data-driven analytical approach. The essence of this method lies in delving into the domain of fractional order differentiation, systematically identifying the most appropriate orders and band positions. This strategy not only enhances the scientific foundation of model construction based on theoretical and empirical data but also significantly improves the model's adaptability and accuracy in practical application scenarios. By taking into account the differential characteristics of spectral data and band sensitivity, this research establishes an accurate and practical model optimization pathway. Thus, while augmenting the scientific integrity of the model, it ensures its effectiveness and reliability in addressing complex real-world application challenges. Figure 4 presents the comprehensive technical roadmap for the modeling process of the mural plaster phosphate Partial Least Squares Regression model, based on Fractional Order Differentiation and spectral indices.

Construction and evaluation of the independent testing set

To validate the generalizability of the proposed three-band spectral index and ensure the impartiality and objectivity of the research findings, an entirely independent testing set was constructed. This testing set comprises 30% of the total dataset, a subset that was not utilized during the training phase of the model nor during the optimization stage of the spectral index. Additionally, the data preprocessing steps for these samples were identical to those used for the samples involved in constructing the spectral index, maintaining consistency in the processing methodology.

The analysis of the independent testing set involved validating the three-band spectral index previously developed using 70% of the sample data. We extracted the same spectral features from the testing data that were used during the construction phase of the three-band spectral index and calculated the spectral index using the same fractional order differentiation degrees. Subsequently, these calculated spectral indices, derived from various fractional order differentiation degrees, served as explanatory variables, with the measured EC values of the independent testing set acting as the response variable. A Partial Least Squares Regression (PLSR) model was then established to rigorously validate the credibility and practicality of the research findings.

Model accuracy evaluation methods

This paper employs accuracy assessment metrics to evaluate the efficacy of the predictive modeling [25, 27, 49]. The computation formulas for R^2 (Coefficient of determination of the calibration dataset), Q2 (Coefficient of determination of the validation dataset), RMSE (Root Mean Square Error), and MAE (Mean Absolute Error) are delineated as follows in Eqs. (9) to (11).

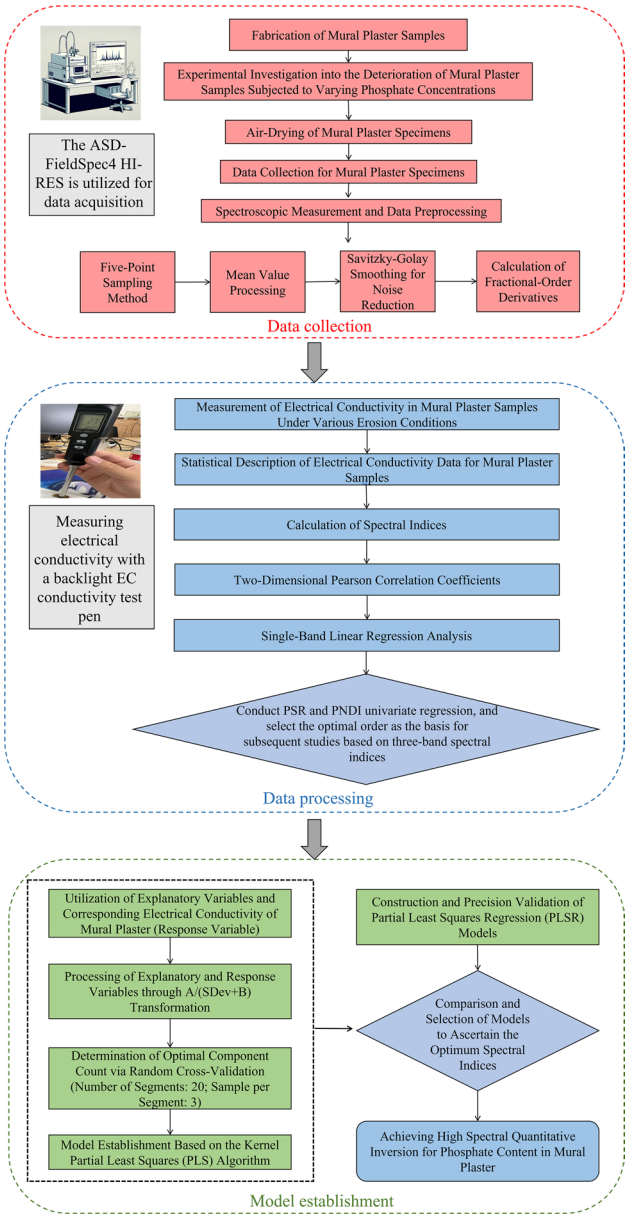

Fig. 4 The comprehensive technical roadmap for the modeling process of the mural plaster phosphate partial least squares regression model, based on fractional order differentiation and spectral indices

$$R^2 = \left(\frac{\sum_{i=1}^{n} (y_i - \bar{y})(z_i - \bar{z})}{\sqrt{\sum_{i=1}^{n} (y_i - \bar{y})^2 \cdot \sum_{i=1}^{n} (z_i - \bar{z})^2}} \right)^2, \quad (9)$$

$$RMSE = \sqrt{\frac{\sum_{i=1}^{n} (y_i - z_i)^2}{n}}, \quad (10)$$

$$MAE = \frac{1}{n} \sum_{i=1}^{n} |y_i - \hat{y}_i|, \quad (11)$$

where n represents the number of mural plaster samples; y_i represents the EC measurement value of the i-th mural plaster sample; $\bar{y}$ represents the average of the measured values of all mural plaster samples; $\hat{y}_i$ represents the predicted value for the i-th sample of Mural Plaster. z_i represents the predicted EC value of the i-th mural plaster sample; $\bar{z}$ represents the average EC predicted value of all mural floor samples; the performance metrics of the model encompass the coefficient of determination for the calibration dataset, denoted by R_c^2, the coefficient of determination for the validation dataset, represented by $RMSE_c$, the coefficient of determination of the validation data set is expressed as Q_v^2, the root mean square error for the validation dataset, articulated as $RMSE_v$, and the mean absolute error, delineated as MAE. Among them, R^2 and Q^2 are used to evaluate the model fitting degree. The closer the value is to 1, the higher the model accuracy. RMSE and MAE are used to evaluate the stability of the model. The closer the value is to 0, the better the RMSE and MAE are.

Calculate

All pertinent computational processes were conducted within a proprietary Graphical User Interface (GUI) based on Anaconda 3, utilizing a Python interactive environment. Furthermore, the construction of the Partial Least Squares Regression (PLSR) model was facilitated through the application of The Unscrambler X 10.4 software. This involved a preprocessing step, specifically the exclusion of 10% of outlier data points from the dataset, to optimize model performance.

Results

Statistical data analysis of electrical conductivity

In this study, to delve into the impact of phosphate erosion on the microstructure of samples, we selected a representative sample (with notably significant deterioration) from multiple samples for detailed examination. Characterizing the micro-porous structure of this chosen sample post-phosphate erosion, and comparing it with that of an unaltered specimen, aimed to unveil the specific effects of phosphate erosion on the material's microstructure. In the experiments, a high-performance

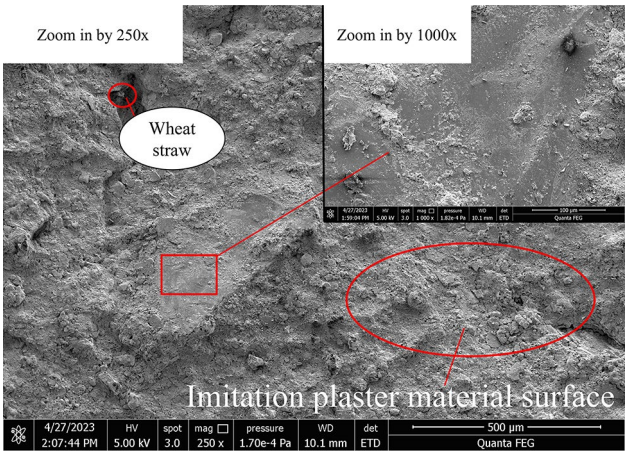

Fig. 5 SEM image of the original sample surface

QUANTA FEG 250 scanning electron microscope (SEM) was utilized as the primary tool for characterization. Leveraging its high-resolution imaging capability, a comparative analysis of the microstructural differences before and after sample erosion was conducted, thus providing crucial microscopic evidence to comprehend the mechanisms behind phosphate erosion.

In this study, by conducting a comparative analysis of the microphotographs of original sample A and phosphate-eroded sample B at various magnifications, as illustrated in Figs. 5 and 6, we observed significant microstructural changes. At a magnification of 2000×, sample A exhibited a uniform texture, whereas sample B displayed distinctly different microfeatures: surfaces dotted with irregularly shaped crystal clusters and presenting an uneven crystal arrangement. Additionally, in sample B, areas of crystal crystallization developed cracks due to stress accumulation, and the material's matrix showed signs of partial delamination and alteration in microform compared to its original state.

These observations stem from a series of experiments designed to investigate the impact of phosphate erosion on the microstructure of cultural heritage materials by simulating the capillary salt ion adsorption and crystallization erosion processes occurring within real mural environments. In contrast to traditional research methods that utilize pre-salted samples under laboratory conditions, the approach adopted in this study more closely approximates actual conditions. This provides more authentic and direct data support for a deeper understanding of the microscopic mechanisms involved in the phosphate erosion process and its effects on the microstructure of cultural heritage materials.

Furthermore, the electrical conductivity (EC) values of the mural plaster samples directly reflect the variance in salt content within the same material, exhibiting a certain degree of variability. As illustrated in Fig. 7, the range of sample EC values spans from 2.06 to 6.43 ms m^{-1}. The

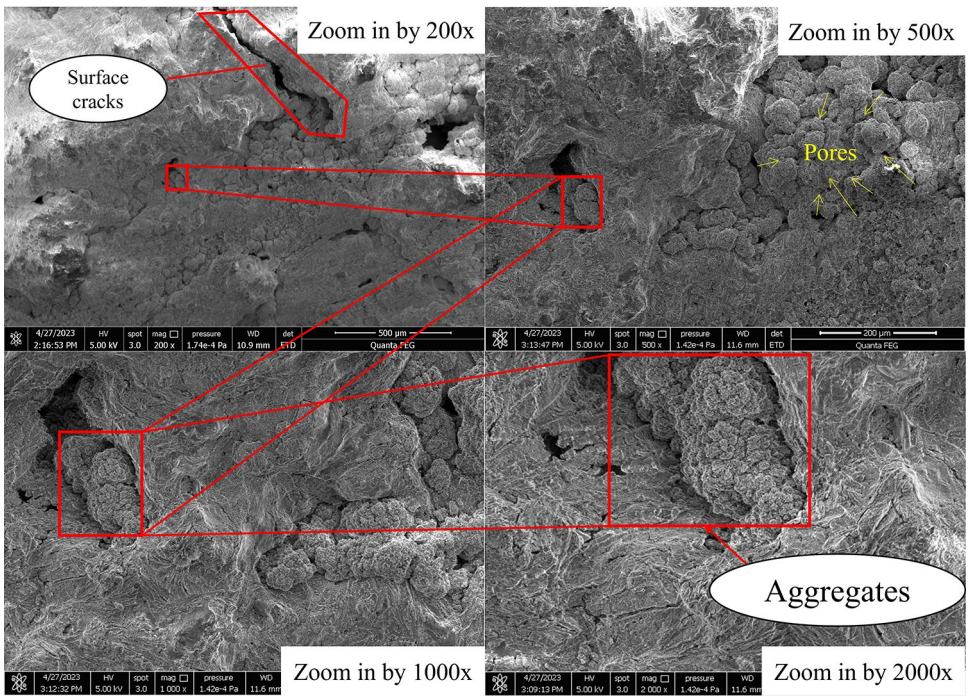

Fig. 6 SEM photographs of the deteriorated sample at various magnifications post-degradation

mean and standard deviation of the sample EC values are calculated to be 3.62 ± 0.88 ms m^{-1}. The first quartile (Q1) and third quartile (Q3) of the data are respectively 2.97 ms m^{-1} and 4.27 ms m^{-1}, indicating that 50% of the sample EC values fall between these two figures. Additionally, the coefficient of variation (CV) stands at 24%, signifying that the relative variability of the EC values is at a moderate level.

Hyperspectral characteristics of simulated mural plaster

The spectral reflectance characteristics of salt-laden mural samples are primarily determined by factors such as material composition, salt concentration, and moisture content. The extraction of characteristic spectral bands supports the inversion of salt content [50, 51]. Figure 8 illustrates the spectral reflectance curves of the samples, where the average spectra of the Mural Plaster samples exhibit consistent shapes and trends, indicating the spectral similarity among the samples. Nevertheless, there are clear differences in reflectance levels among samples with varying salt concentrations, reflecting the influence of salt concentration on spectral reflectance properties.

Observations in Fig. 8 demonstrate that the spectral analysis of the Mural Plaster samples reveals stable reflectance and distinct characteristic absorption bands, predominantly influenced by the interactions between organic matter and minerals. Particularly at the characteristic wavelengths of clay minerals, such as 1400 nm, 1900 nm, and 2200 nm, more pronounced absorption bands are observed. These peaks reflect the vibrational characteristics of water and Al–OH groups in clay minerals [52], providing essential information for the identification and analysis of mineral components in Mural Plaster samples. Moreover, spectral reflectance typically decreases and then increases with rising salt concentrations, aligning with the findings of Guo et al. However, this pattern changes significantly under conditions of

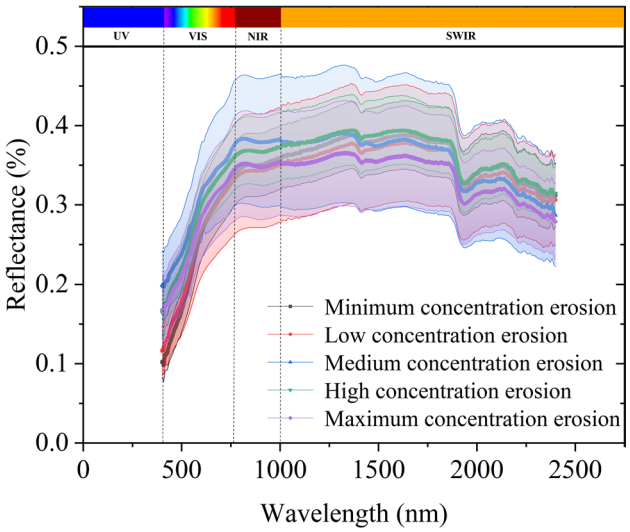

Fig. 8 Spectral reflectance curves of simulated mural plaster samples under various salt erosion concentrations

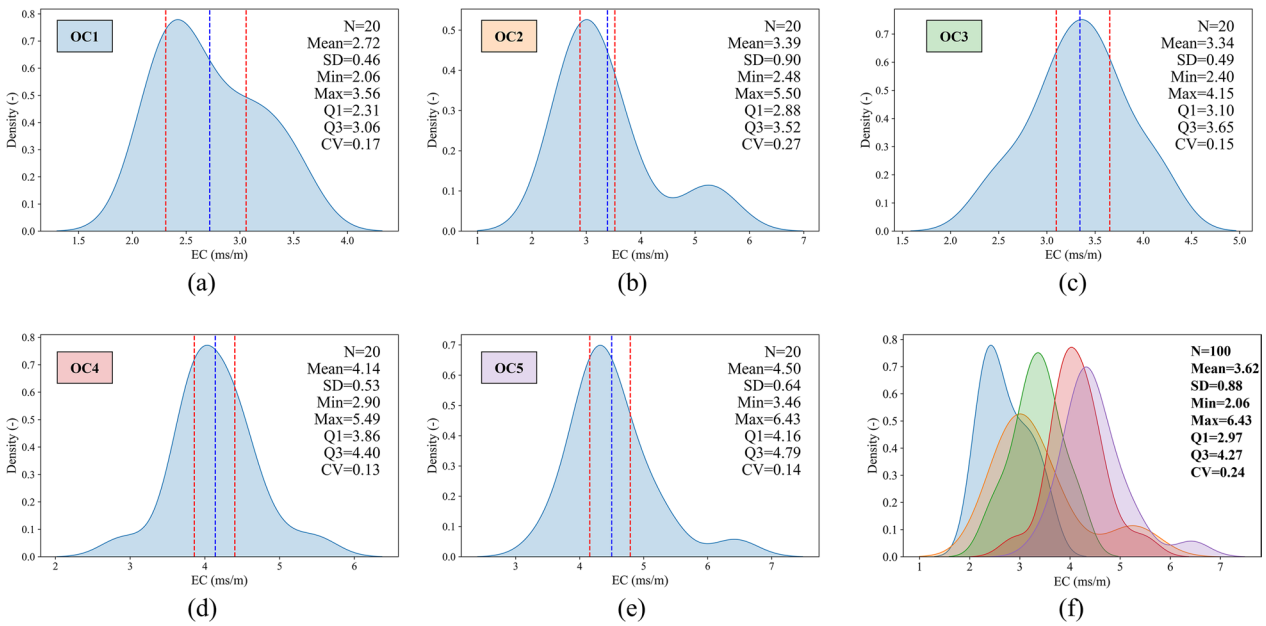

Fig. 7 Presents a statistical analysis of the mural plaster EC values, where **a**–**e** respectively depict the data statistical descriptions under five different conditions, including density distribution, mean, standard deviation (SD), minimum value (Min), maximum value (MAX) first quartile (Q1), third quartile (Q3), and coefficient of variation (CV). **f** Represents a comprehensive statistical analysis of all aggregated data

highest concentration erosion, where a marked decline in spectral reflectance occurs. This may be attributed to several factors. At the highest concentration of erosion, the mural samples experience the greatest degree of deterioration, increasing their porosity and surface roughness, thereby enhancing their water-absorptive properties [53], changes that might not be as apparent under moderate or low concentration conditions. Therefore, it is plausible that the observed decrease in reflectance under extreme erosion conditions could be due to increased sample moisture. Additionally, asymmetric absorption troughs appear near 1420 nm and 1940 nm, with the latter showing more significant depth and breadth. The former is due to specific vibrational absorption characteristics of moisture in the samples at 1420 nm [28], where the presence of phosphates may indirectly influence the formation and characteristics of this absorption valley by affecting the soil's moisture adsorption and retention properties. The latter likely results from the characteristic absorption features of phosphates in the short-wave infrared region (SWIR), associated with the vibrational modes of phosphate–oxygen bonds in their molecular structure [54].

Furthermore, in exploring the effects of varying salt concentration erosions on the spectral reflectance of mural samples, we noted that reflectance typically decreases and then increases with the escalation of salt concentration. However, this pattern undergoes a significant alteration under the conditions of highest concentration erosion, where a notable decline in spectral reflectance is observed. This phenomenon is likely due to a combination of two factors. Firstly, under the conditions of maximum concentration erosion, the mural samples undergo the most extensive deterioration, increasing their porosity and surface roughness, which in turn enhances their water-absorptive capacity [53]; such changes are less pronounced at moderate or low concentration levels. Secondly, in natural environments, phosphates also tend to absorb surrounding moisture, which increases the sample's humidity. Typically, an increase in soil humidity results in a reduction in soil reflectance, particularly noticeable at lower moisture levels [55]. Therefore, we hypothesize that the observed reduction in reflectance under conditions of highest concentration erosion could be attributed to an increase in sample humidity.

Characteristics of spectra with different FOD orders

Given the rich high-dimensional information in hyperspectral data and the difficulty in capturing sensitive bands and features [56], the FOD calculation method delineated in "Modeling using a single two-band spectral index (PNDI)" section was utilized on the samples. This method allows for the control of differential step length, thereby enhancing the accuracy of salt content detection. Following the methodology proposed by Zhang et al. [27], the interval and step length were set at [0–2] and 0.1, respectively. Figure 9 illustrates the average spectrum of the Mural Plaster samples.

Following Fractional-Order Derivative (FOD) processing, Mural Plaster samples exhibit three distinct hygroscopic valleys around 1400 nm, 1900 nm, and 2200 nm, indicating an enhancement in water absorption characteristics [28]. This alteration is associated with an increase in porosity and surface roughness post-phosphate treatment, augmenting the sample's capacity for water absorption. Additionally, the inherent hygroscopic nature of phosphates may also contribute to elevated sample moisture [53]. Therefore, the moisture absorption properties in these wavelength regions could potentially encompass phosphate-related information. With increasing orders of FOD processing, the spectral curve morphology tends to decrease. At the 0.5 order, the reflectance across the entire spectral wavelength fluctuates around values from 0 to 0.03, with the onset of negative values; by the 0.8 order, the reflectance across the entire spectral wavelength has already fallen below 0.1. Following the 0.6 order differential spectrum, a plethora of easily observable curve fluctuations emerge, amplifying differences between various spectra, yet the increment in order does not permit this divergence to continue to expand. After the 1.1 order, this trend gradually moderates, and post-1.4 order, the spectral curve contours become blurred and intermingled, indicating that at higher differential orders, the spectral curve contours are progressively obscured, and the curves lose clear differential intervals between them. In establishing a electrical conductivity inversion model within Mural Plaster, employing fractional-order differential techniques effectively broadens the difference between spectral data, enhancing spectral feature information, thus improving the model's accuracy and robustness. This can be elucidated by the mathematical theory behind the Grünwald–Letnikov (G–L) method. Given the presence of peaks and valleys of certain widths in reflectance, when the sampling step is smaller than these widths, such differences are amplified during computation, thereby enhancing spectral information. Inevitably, the differentiation operation may lead to noise significantly different from adjacent bands, or short-interval reflectance peaks and valleys being amplified again, thereby introducing high-frequency noise [27].

Spectral index analysis

Modeling using a single two-band spectral index (PNDI)

In this study, we delve into the application of Fractional Order Derivative (FOD) within the realm of

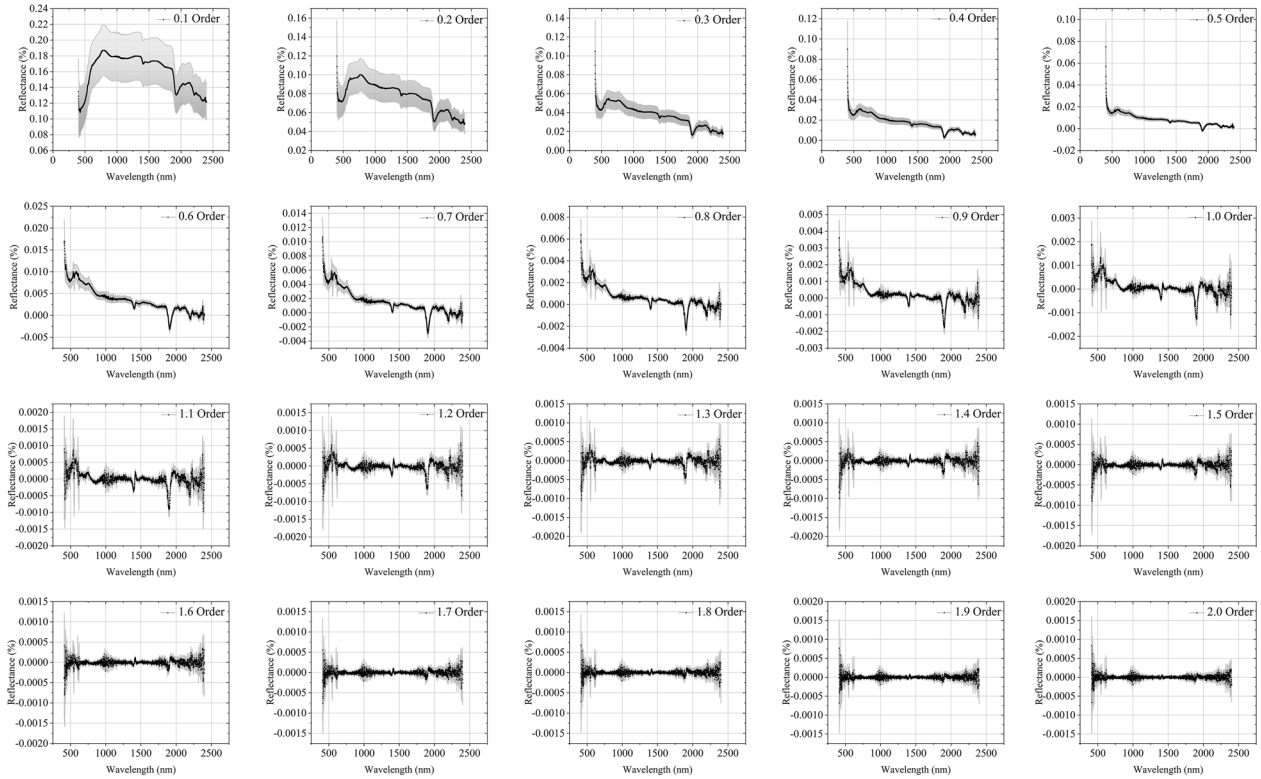

Fig. 9 The average fractional-order derivative spectra of mural plaster samples. The order interval ranges from 0 to 2, with a step size of 0.1. The black curve represents the mean spectrum of the mural plaster samples, while the grey shading denotes its standard deviation

hyperspectral remote sensing technology, specifically aimed at optimizing the spectral estimation of electrical conductivity in Mural Plaster. Through experimental analysis, we employed various FOD orders to calculate the Mural Plaster's two-band spectral index (Phosphorus Normalized Difference Index, PNDI), with the objective of identifying the optimal FOD order that maximizes the correlation between PNDI and electrical conductivity.

From Fig. 10 and Table 1, it can be observed that the Maximum Absolute Correlation Coefficient (MACC) between PNDI and electrical conductivity exhibits a trend of initial increase followed by a decrease as the order of the Fractional Order Derivative (FOD) increases. In Fig. 10, the depth of color in the bands represents the absolute values of the correlation coefficients, with darker colors indicating higher absolute values and lighter colors indicating lower absolute values. In Fig. 11 the bands denote scatter density calculated through Gaussian Kernel Density Estimation (KDE). Here, the variation in color intensity reflects different levels of data point density: darker areas signify a higher concentration of data points, while lighter areas indicate a sparser distribution. Furthermore, subsequent charts employ the same representational method and principles. Notably, at the 0.6 order, the MACC reaches its zenith at 0.652, indicating that FOD processing at this order is most effective in enhancing the correlation between PNDI and electrical conductivity.

In the process of further in-depth analysis, we paid particular attention to the characteristic wavelengths that exhibited the strongest correlation with electrical conductivity and utilized these wavelengths to construct a spectral index model for estimating electrical conductivity. A meticulous evaluation of the data presented in Fig. 11 and Table 1 reveals that when employing a singular two-band spectral index (PNDI) for model construction, the Fractional Order Derivative (FOD) processing at the 0.3 order enabled the model to achieve the highest determination coefficient ($Q^2 = 0.728$), significantly enhancing the accuracy of electrical conductivity estimation. Moreover, through comparative analysis of FOD processing across the ranges of 0.1 to 0.9 and 1 to 2 orders, we discovered that the lower orders (0.1 to 0.9) of fractional-order derivatives are more effective in the estimation of electrical conductivity. This phenomenon unveils a critical observation: higher-order FOD processing tends to introduce excessive noise, leading to instability and

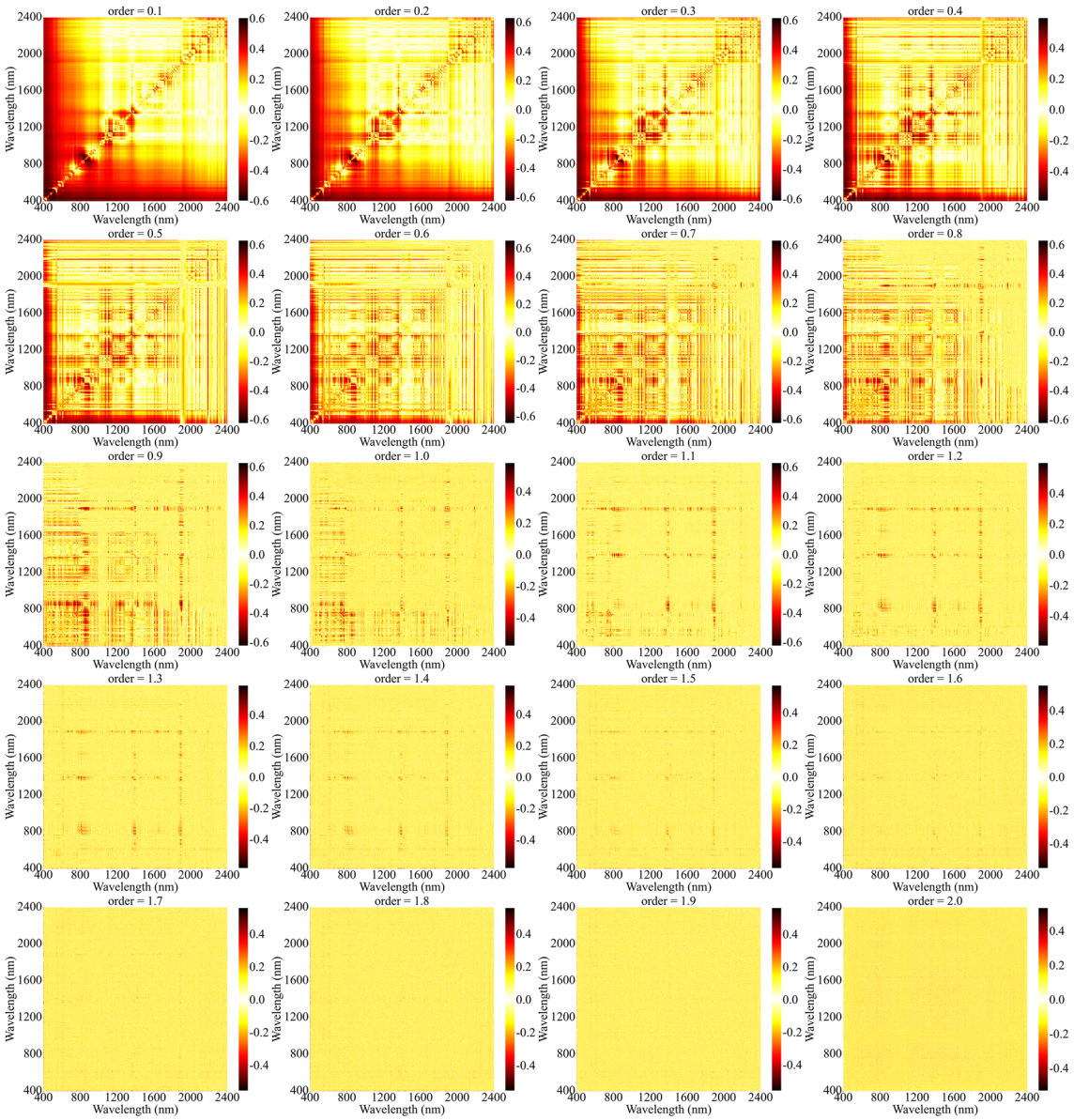

Fig. 10 Correlation coefficient between electrical conductivity in mural plaster and the two-band spectral index (PNDI)

reduced accuracy in estimation outcomes [32]. This effect might be attributed to high-order FOD amplifying non-essential variability within the hyperspectral data, which bears a weaker actual relation to the target variable (i.e., electrical conductivity). From the perspective of hyperspectral remote sensing expertise, this finding underscores the importance of selecting an appropriate FOD order for spectral feature extraction and substance content estimation. When applying fractional-order derivatives to hyperspectral data, a balance must be struck between signal enhancement and noise control to ensure the stability and accuracy of the final model. Low-order FOD processing, to some extent, provides a more optimal balance point, as it is capable of effectively extracting features highly sensitive to the target variable while controlling the noise that might be introduced by excessively high-order derivatives [57, 58].

The univariate regression analysis conducted on the validation dataset, as displayed in Fig. 11, allows us to observe the performance of linear regression models based on the two-band spectral index (PNDI) across different FOD orders. This analysis encompasses FOD orders of 0.3, 0.8, 0.2, 0.4, 0.9, and 1.2, with the model

Table 1 Employing linear regression, we have derived the estimation results for the characteristic wavelengths of electrical conductivity in mural plaster and the two-band spectral index (PNDI)

Order	MACC	R_a (nm)	R_b (nm)	Calibration dataset			Validation dataset		
				R_c^2	$RMSE_c$	MAE_c	Q_v^2	$RMSE_v$	MAE_v
0.1	0.6	862	846	0.567	0.461	0.392	0.645	0.466	0.395
0.2	0.625	887	844	0.57	0.457	0.377	0.698	0.417	0.373
0.3	0.613	886	841	0.509	0.487	0.409	0.728	0.394	0.312
0.4	0.593	894	825	0.578	0.464	0.39	0.667	0.406	0.321
0.5	0.627	879	825	0.592	0.455	0.376	0.537	0.463	0.399
0.6	0.652	879	825	0.627	0.452	0.378	0.601	0.422	0.334
0.7	0.628	879	824	0.587	0.466	0.384	0.544	0.472	0.377
0.8	0.626	401	449	0.677	0.365	0.28	0.699	0.495	0.439
0.9	0.624	401	462	0.477	0.489	0.389	0.655	0.455	0.368
1	0.579	798	770	0.47	0.522	0.457	0.437	0.515	0.455
1.1	0.625	1407	847	0.563	0.471	0.408	0.507	0.495	0.43
1.2	0.596	1407	815	0.4	0.51	0.446	0.651	0.518	0.48
1.3	0.587	2186	1051	0.47	0.506	0.432	0.39	0.499	0.423
1.4	0.582	401	1370	0.479	0.502	0.416	0.53	0.482	0.41
1.5	0.566	401	1370	0.519	0.481	0.405	0.47	0.518	0.422
1.6	0.549	1369	403	0.493	0.485	0.401	0.357	0.581	0.513
1.7	0.557	402	1764	0.496	0.498	0.419	0.393	0.588	0.511
1.8	0.555	401	1764	0.38	0.511	0.434	0.559	0.575	0.506
1.9	0.559	401	1764	0.39	0.507	0.432	0.556	0.577	0.495
2	0.532	401	1409	0.461	0.504	0.429	0.437	0.534	0.465

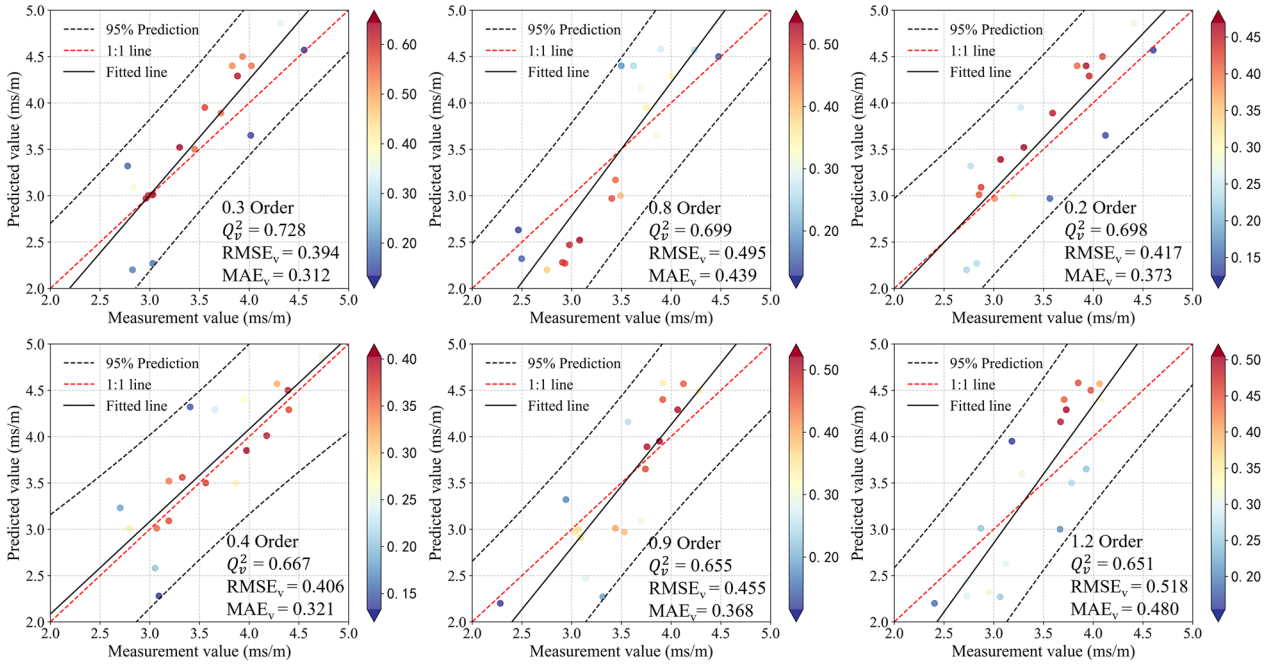

Fig. 11 Based on the univariate regression scatter plots of the two-band spectral Index (PNDI) within the validation dataset, encompassing the orders ranked within the top six for model accuracy

accuracies of these orders ranking among the top six across all tested orders. This discovery reveals that employing these FOD orders, which exhibit higher model accuracies, might be the optimal strategy for constructing spectral inversion models for electrical conductivity in Mural Plaster. The advantage of this approach lies in its ability to enhance target spectral features while effectively suppressing noise by selecting specific fractional-order derivatives, thereby demonstrating higher efficiency and accuracy in extracting spectral information closely related to electrical conductivity [59]. In summary, when establishing a spectral inversion model for electrical conductivity in Mural Plaster, opting for spectral analysis with FOD orders that rank in the top six in terms of linear regression model accuracy might be the best choice.

Modeling using a single two-band spectral index (PSR)

Simultaneously, within the experimental framework, varying orders of Fractional Order Derivative (FOD) were utilized to compute the two-band spectral index (PSR), with the aim of identifying the optimal FOD order that would maximize the correlation between PSR and electrical conductivity, thereby achieving the greatest possible association between PSR and the electrical conductivity.

From Fig. 12 and Table 2, it can be observed that the Maximum Absolute Correlation Coefficient (MACC) between PSR and electrical conductivity also exhibits a trend of initially increasing and then decreasing with the rise in FOD orders, mirroring the trend observed with PNDI. Notably, the MACC reaches its apex at 0.653, similarly at the 0.6 order.

In the continuation of our in-depth analysis, through the data presented in Fig. 13 and Table 2, we discovered that when constructing a model using a singular two-band spectral index (PSR), the application of Fractional Order Derivative (FOD) processing at the 0.3 order enabled the model to achieve the highest determination coefficient ($Q^2 = 0.728$), significantly enhancing the accuracy of electrical conductivity estimation. Furthermore, through comparative analysis of FOD processing across the ranges of 0.1 to 0.8 and 1 to 2 orders, we identified that lower orders (0.1 to 0.8) of fractional-order derivatives prove to be more effective in the estimation of electrical conductivity. The univariate regression analysis conducted on the validation dataset, as depicted in Fig. 13, allows us to observe the performance of linear regression models based on the two-band spectral index (PSR) across different FOD orders. This analysis includes FOD orders of 0.3, 0.7, 0.8, 0.2, 0.1, and 0.4, with the model accuracies of these orders ranking among the top six across all tested orders.

Partial least squares regression modeling of the two-band spectral index

Within the framework of this study, the selection of specific three-band wavelengths no longer solely relies on the outcomes of previous research but employs a data-based analytical approach. Initially, a high-precision comprehensive analysis was conducted through the modeling of two-band spectral indices using the Partial Least Squares Regression (PLSR) model. By analyzing the spectral indices that exhibited the best performance in the top six orders of univariate regression, these indices were utilized as explanatory variables for conducting Partial Least Squares Regression (PLSR) analysis on electrical conductivity. Ultimately, as depicted in Fig. 14, the accuracy of the PSR–PLSR modeling surpassed that of the PNDI–PLSR model, achieving a determination coefficient (Q^2) of 0.759.

Employing single three-band spectral index modeling (PTSR)

The correlation coefficients between the three-band spectral index at different FOD orders and the electrical conductivity in Mural Plaster are presented in Fig. 15 and Table 3. The horizontal and vertical axes denote the spectral bands. Table 3 lists the Maximum Absolute Correlation Coefficient (i.e., the greater value between the maximum positive and maximum negative correlation coefficients). Through a cumulative comparison method, the maximum absolute correlation coefficient of the three-band spectral index has increased by 5.32% compared to the PSR, indicating that the correlation between the spectral index and electrical conductivity is significantly enhanced after employing a three-band combination for fractional-order derivative processing.

Furthermore, as derived from Fig. 16, compared to the univariate regression model of the two-band spectral index (PSR) within the validation dataset, the model accuracy of the three-band spectral index has also seen a significant enhancement. This finding not only attests to the superiority of the three-band spectral index in modeling electrical conductivity but also underscores the importance of meticulous spectral feature selection and appropriate mathematical processing techniques in hyperspectral remote sensing analysis. The experimental results further emphasize that through in-depth analysis and precise processing of spectral data, more representative spectral indices can be extracted. This provides a new theoretical basis and methodological guidance for the application and development of hyperspectral remote sensing technology.

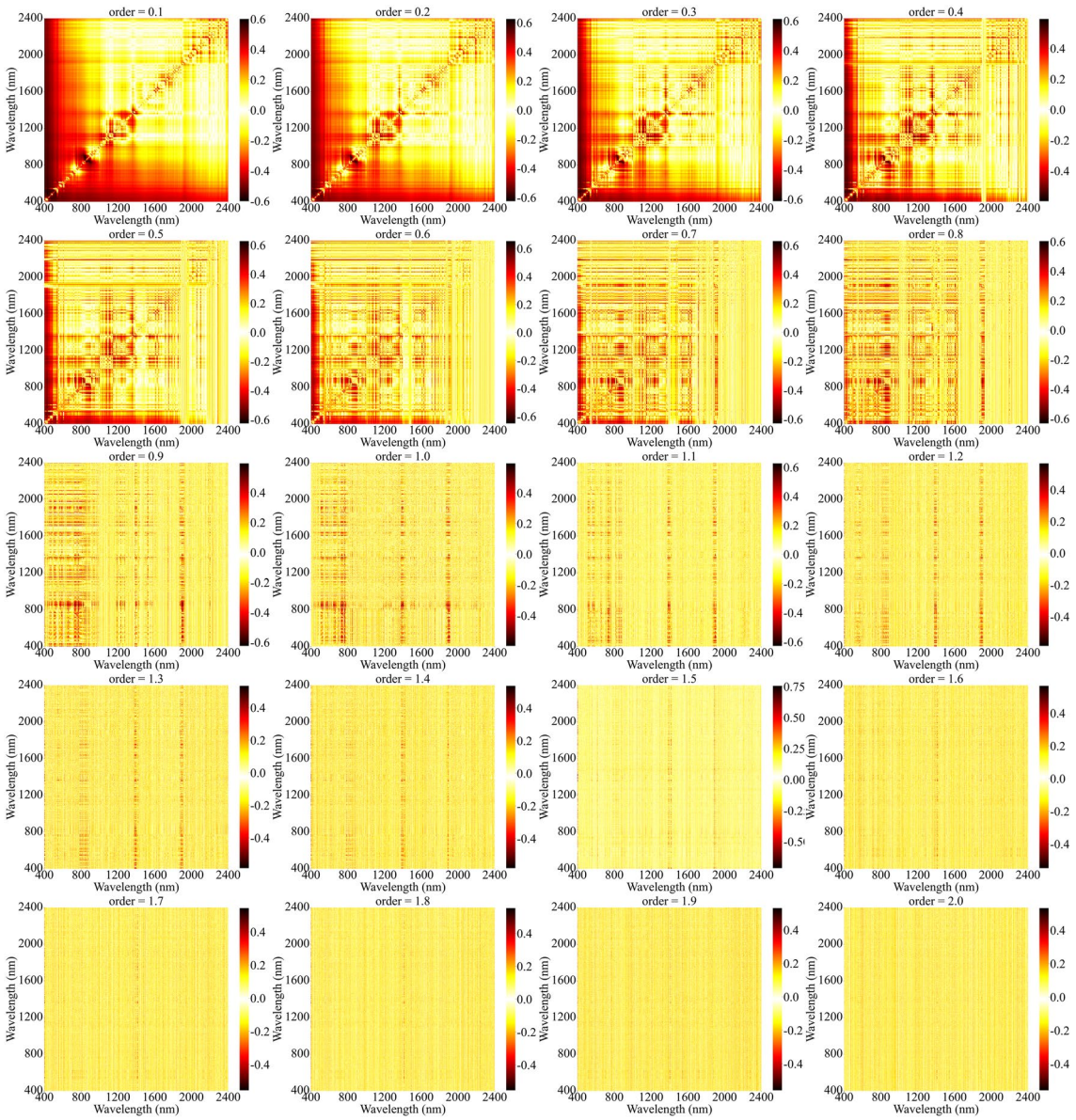

Fig. 12 Correlation coefficient between electrical conductivity in mural plaster and the two-band spectral index (PSR)

Predictive model for electrical conductivity in mural plaster based on fractional order differential combined with novel spectral indices

In this research, we have constructed a high-precision model for monitoring electrical conductivity in Mural Plaster using Fractional Order Derivative (FOD) technology combined with the three-band spectral index (PTSR). Figure 17 showcases the optimal Mural Plaster electrical conductivity monitoring model established based on FOD spectra and three-band spectral index (PTSR) utilizing validation set data. Through thorough analysis, the PTSR–PLSR model demonstrated a significant performance enhancement compared to the previous PNDI–PLSR and PSR–PLSR models, specifically reflected in a determination coefficient (Q^2) of 0.815 and a reduction in Root Mean Square Error (RMSE) to 0.327, marking an accuracy improvement of 10.4% and 7.38%, respectively, over the PNDI–PLSR and PSR–PLSR models. These results not only affirm the high accuracy and reliability of the PTSR–PLSR model in monitoring electrical conductivity in Mural Plaster but also highlight the potential application of FOD

Table 2 Employing linear regression, we have derived the estimation results for the characteristic wavelengths of electrical conductivity in mural plaster and the two-band spectral index (PSR)

Order	MACC	R_a (nm)	R_b (nm)	Calibration dataset			Validation dataset		
				R_c^2	$RMSE_c$	MAE_c	Q_v^2	$RMSE_v$	MAE_v
0.1	0.601	846	862	0.567	0.461	0.392	0.645	0.466	0.396
0.2	0.625	844	887	0.57	0.457	0.377	0.698	0.417	0.373
0.3	0.613	841	886	0.509	0.487	0.409	0.728	0.394	0.312
0.4	0.598	427	481	0.54	0.465	0.378	0.626	0.485	0.419
0.5	0.627	879	825	0.591	0.456	0.377	0.538	0.463	0.399
0.6	0.653	879	825	0.627	0.452	0.378	0.604	0.420	0.333
0.7	0.630	401	449	0.607	0.398	0.306	0.728	0.457	0.383
0.8	0.633	401	449	0.678	0.365	0.279	0.700	0.494	0.441
0.9	0.624	918	879	0.616	0.448	0.371	0.452	0.526	0.442
1	0.599	750	848	0.455	0.492	0.420	0.597	0.539	0.475
1.1	0.629	748	848	0.579	0.465	0.393	0.459	0.571	0.442
1.2	0.567	1403	848	0.499	0.499	0.419	0.490	0.537	0.466
1.3	0.587	401	1370	0.556	0.465	0.378	0.457	0.529	0.442
1.4	0.582	401	1370	0.478	0.502	0.417	0.530	0.482	0.409
1.5	0.755	402	1394	0.246	0.609	0.521	0.270	0.574	0.496
1.6	0.567	491	2049	0.434	0.518	0.445	0.339	0.558	0.465
1.7	0.556	402	1764	0.494	0.499	0.420	0.391	0.589	0.513
1.8	0.555	401	1764	0.379	0.511	0.434	0.559	0.575	0.506
1.9	0.559	401	1764	0.390	0.507	0.432	0.556	0.577	0.495
2	0.558	401	1764	0.396	0.504	0.431	0.540	0.587	0.506

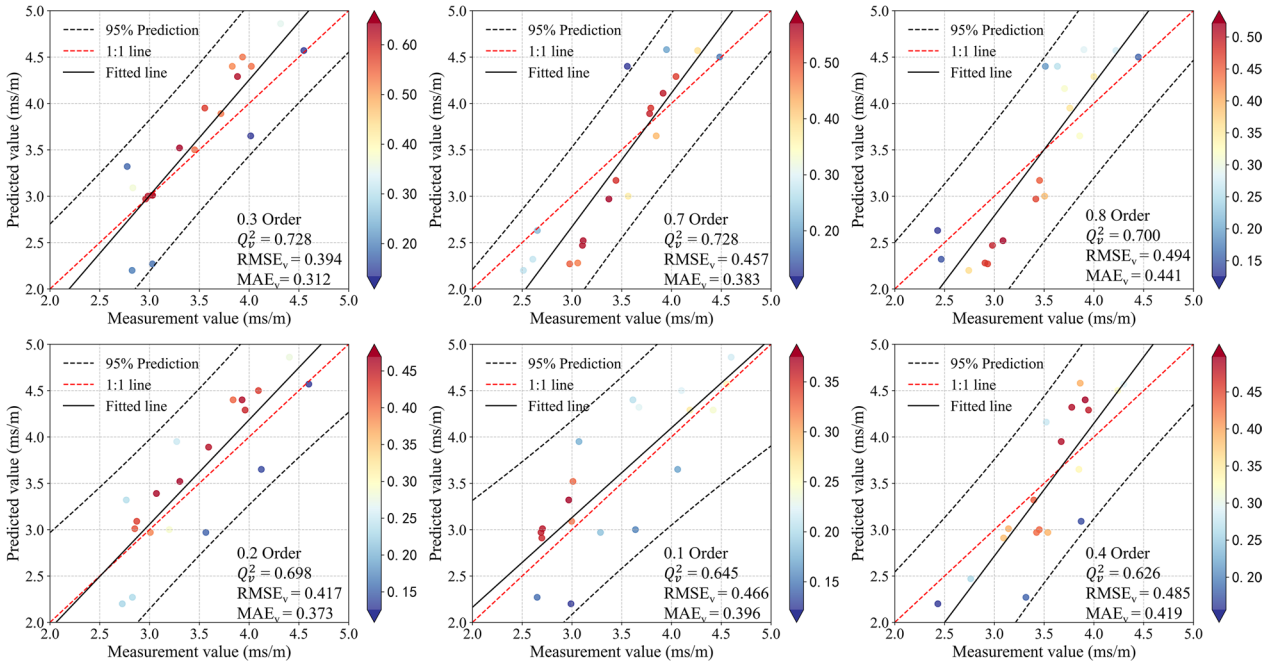

Fig. 13 Based on the univariate regression scatter plots of the two-band spectral index (PSR) within the validation dataset, encompassing the orders ranked within the top six for model accuracy

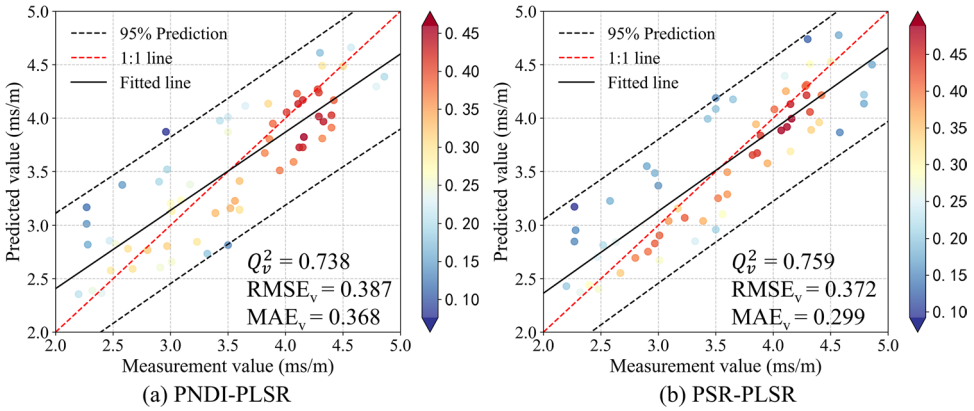

Fig. 14 The optimal mural plaster electrical conductivity monitoring model established based on FOD spectra and two-band spectral indices (Utilizing validation set data): **a** PNDI–PLSR model **b** PSR–PLSR model

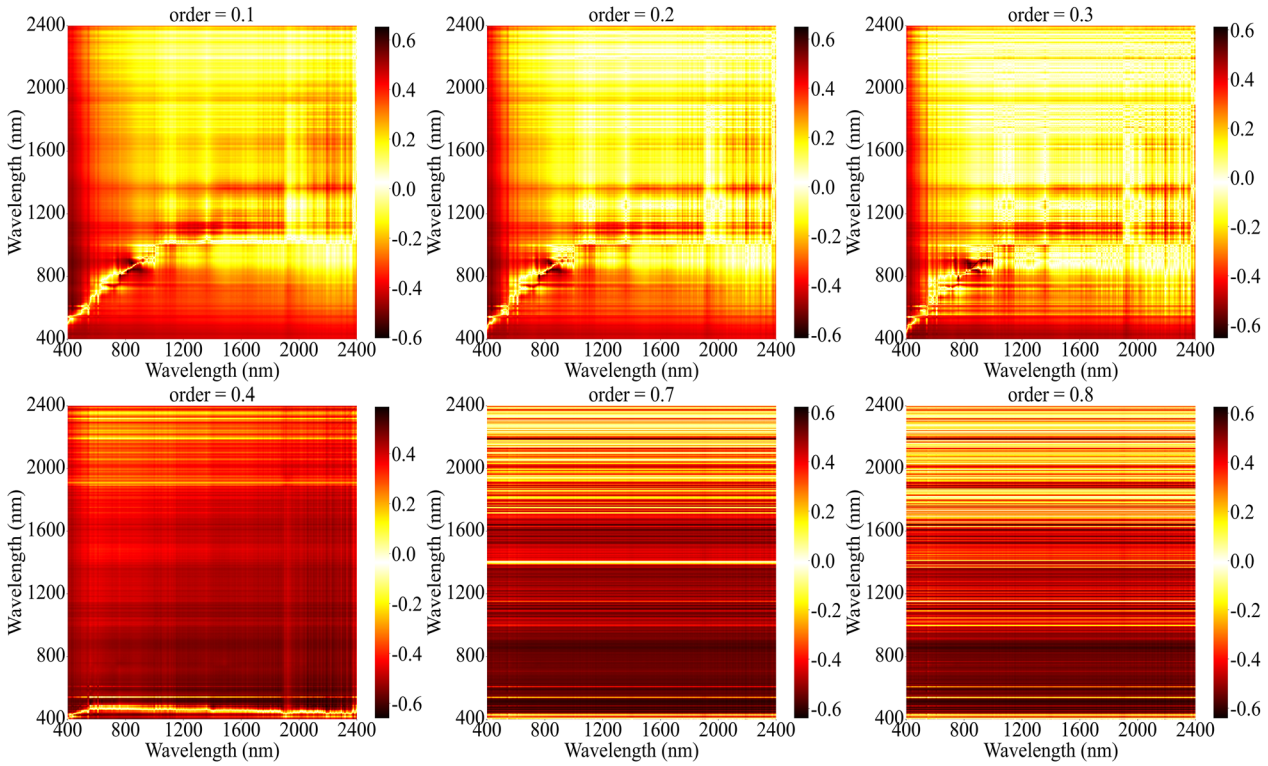

Fig. 15 Correlation coefficient between electrical conductivity in mural plaster and the three-band spectral index (PTSR)

technology and the novel three-band spectral index in the field of hyperspectral remote sensing monitoring.

Evaluation and validation of the three-band spectral index on an independent testing set

In "Predictive model for electrical conductivity in mural plaster based on fractional order differential combined with novel spectral indices" section, we developed a predictive model for the electrical conductivity in Mural Plaster based on a novel three-band spectral index integrated with fractional-order differentiation. While this model performed commendably on the training set, the absence of an independent testing set to validate the effectiveness of the three-band spectral index limited our ability to impartially assess the model's performance. Consequently, to thoroughly evaluate its generalization capabilities and ensure the unbiased nature of our research outcomes, we conducted validation work on an

Table 3 Employing linear regression, we have derived the estimation results for the characteristic wavelengths of electrical conductivity in mural plaster and the two-band spectral index (PTSR)

Order	MACC	R_a (nm)	R_b (nm)	R_c (nm)	Calibration dataset			Validation dataset		
					R_c^2	$RMSE_c$	MAE_c	Q_v^2	$RMSE_v$	MAE_v
0.1	0.653	815	836	846	0.627	0.427	0.364	0.73	0.417	0.336
0.2	0.65	815	829	844	0.631	0.427	0.365	0.653	0.423	0.368
0.3	0.654	957	904	841	0.553	0.476	0.392	0.557	0.491	0.437
0.4	0.66	2194	482	427	0.508	0.455	0.366	0.767	0.441	0.356
0.7	0.639	2057	449	401	0.615	0.394	0.305	0.753	0.436	0.364
0.8	0.641	2057	449	401	0.687	0.360	0.277	0.722	0.476	0.423

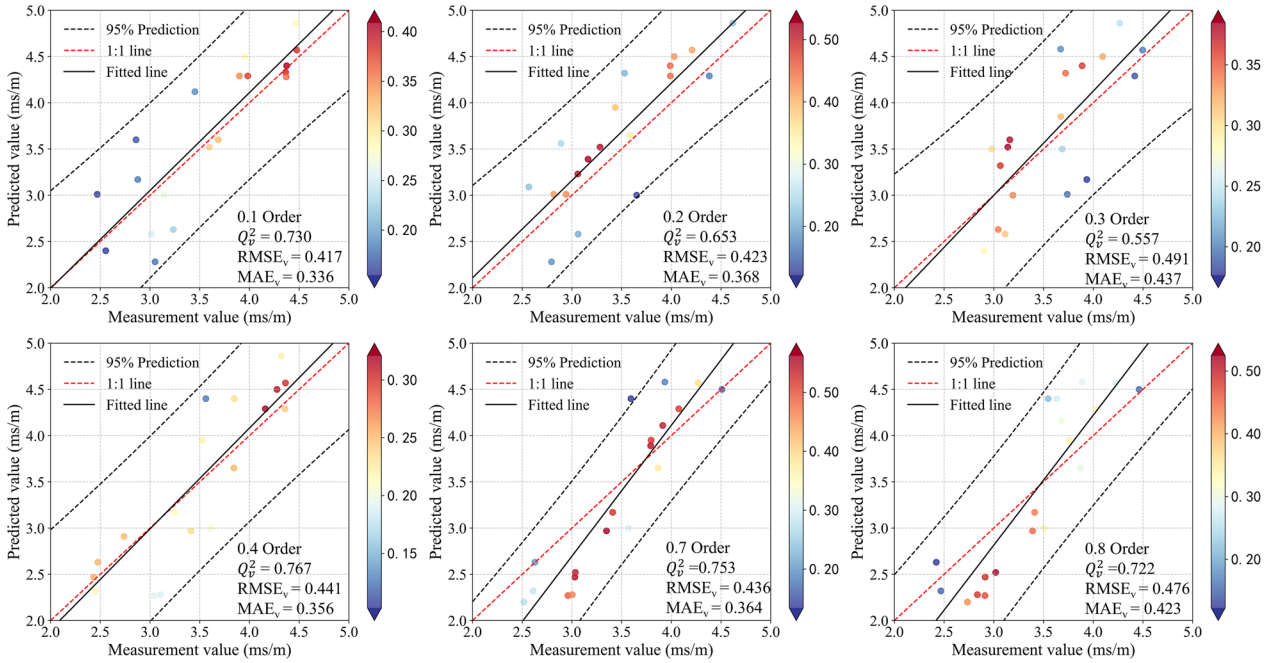

Fig. 16 Univariate regression scatter plot of the two-band spectral index (PTSR) based on the validation dataset

independent testing set, a critical step in understanding and confirming the efficacy of the three-band spectral index.

As illustrated in Fig. 18, the Partial Least Squares Regression (PLSR) model constructed using the three-band spectral index achieved a prediction accuracy of 0.716 on an independent testing set. Although this result is lower than the 0.815 prediction accuracy obtained using 70% of the sample data, it provides an important unbiased estimate, highlighting the true performance of the three-band spectral index when faced with unknown data. This finding is particularly significant as it demonstrates the robust generalization ability of the three-band spectral index, maintaining a reliable predictive efficacy in environments different from the training data.

Furthermore, the evaluation results from the independent testing set have also revealed several factors that might affect model performance. Firstly, the data in the testing set may possess characteristics distinct from those in the training and validation sets, a diversity that is one potential cause of the observed decline in model performance. Secondly, any predictive model may encounter generalization errors when faced with new datasets, particularly when the distribution of these data deviates from that of the training data.

Therefore, the use of an independent testing set is not only a crucial step in evaluating the generalization capabilities of the three-band spectral index but also an integral component of refining the model evaluation system. This method of assessment enhances our

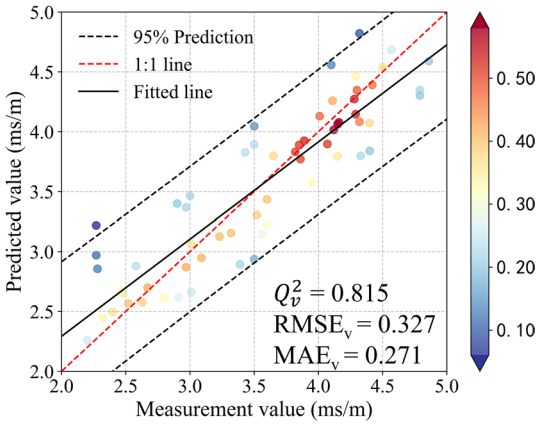

Fig. 17 The optimal mural plaster electrical conductivity monitoring model established based on FOD spectra and three-band spectral index (PTSR) using validation set data

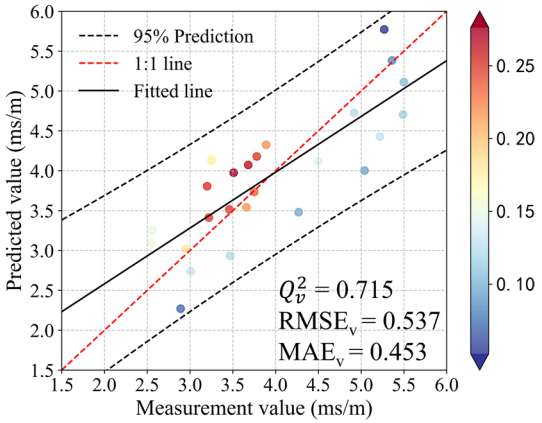

Fig. 18 Partial least squares regression (PLSR) model based on the three-band spectral index on an independent testing set

understanding of the model's performance in real-world application settings, providing valuable data support for further optimization of the model and validation of new spectral indices. Through this approach, we can more objectively assess the practical value and effectiveness of the three-band spectral index in real applications, ensuring the objectivity and impartiality of our research results.

Discussion

Performance analysis of fractional order derivative methods in monitoring electrical conductivity in mural plaster

The surface and internal structure of Mural Plaster undergo significant changes under the influence of salt damage, with variations in porosity and surface roughness directly correlated to the extent of salt damage, significantly impacting the collection and analysis of spectral data [38]. Considering the effects of salt damage on Mural Plaster, especially its impact on porosity and surface roughness, this study obtains samples with varying physical properties by simulating different salt concentration environments, thereby facilitating the collection and analysis of spectral data.

For the preprocessing of hyperspectral data, it is imperative not only to possess the capability to enhance the sensitivity of the spectral data under examination but also to have the potential to optimize the quantitative effects of the model [60, 61]. Therefore, selecting appropriate spectral preprocessing techniques is crucial in the spectral analysis of soil properties. The fractional order differentiation method is recognized for its ability to reduce baseline and background noise, enhance spectral characteristics of soil properties, and improve the accuracy of validation models [25, 26, 62]. Based on this premise, this study endeavors to investigate the efficacy of the fractional order differentiation method in monitoring electrical conductivity within Mural Plaster samples and to conduct a more systematic analysis thereof. Concurrently, researchers have commenced the application of the FOD method in studies on soil properties [29, 30].

In this study, we employed a step of 0.1 order to examine the variations of Fractional Order Derivative (FOD) and found that the utilization of FOD unveils more implicit information pertinent to the target variable. As observable from Fig. 9, the morphology of the spectral curve diminishes with an increase in the FOD processing order. At the 0.5 order, the reflectance corresponding to the entire spectral wavelength fluctuates around values from 0 to 0.03, with the inception of negative values; by the 0.8 order, the reflectance corresponding to the entire spectral wavelength has already dropped below 0.1. Following the 0.6 order differential spectrum, a plethora of easily observable curve undulations emerge, amplifying the differences between various spectral lines. However, the increment in order does not permit this variance to continue to expand; after the 1.1 order, this trend gradually moderates, and post-1.4 order, the spectral curve contours become blurred and overlapped, indicating that at higher differential orders, the outlines of spectral curves are progressively obscured, and the curves lose clear differential intervals between them. Thus, obtaining FOD spectra with a high signal-to-noise ratio is crucial for the analysis and estimation of electrical conductivity in Mural Plaster.

Based on the correlation analysis (Figs. 10, 12, 15, and Tables 1, 2, 3), the electrical conductivity data and FOD spectra exhibit a good correlation within the 0.1–0.9

order FOD range, particularly within the near-infrared light range of 825–887 nm. When conducting univariate linear regression, it was found that the model performance reached its optimum at the 0.3 order differential processing for both PSR and PNDI data, with an R^2 of 0.728 for each. These experimental results highlight the significance of the near-infrared range of 825–887 nm for phosphate research and also demonstrate that fractional order differentiation enhances the accuracy of modeling. Therefore, the spectral range of 0.1–0.9 orders outperforms those at other FOD intervals in improving the spectral response to Mural Plaster electrical conductivity and in uncovering potential information.

Predictive performance and application of the hyperspectral feature inversion model for electrical conductivity in mural plaster based on the three-band spectral index

Optimal spectral indices, calculated based on sensitive wavelengths related to characteristic properties, can readily detect subtle absorption peaks and are utilizable for predicting diverse soil attributes [43, 63, 64]. Numerous algorithms have been devised to optimize two-band combinations for capturing soil characteristics of interest, yet algorithms for band optimization involving three wavelengths remain elusive. Drawing on the research by Lv et al. [44], we constructed a new three-band spectral index (PTSR) based on the SR (simple ratio) form. Our findings (illustrated in Figs. 15 and 17, and Table 3) demonstrate that the introduction of a third wavelength enhances the sensitivity of the SR, indicating a discernible disparity between two-band and three-band indices. Our results parallel those reported by Chen et al. [32], who noted that three-band indices constructed using band optimization algorithms surmounted issues of collinearity and redundancy in hyperspectral data. Unlike their approach, our study does not merely rely on previous research outcomes but employs a data-driven analysis method. The crux of this methodology lies in delving into the realm of fractional order differentiation, systematically selecting the most suitable orders and wavelength positions. This strategy not only elevates the scientific foundation of model construction based on theory and empirical data but also significantly boosts the model's adaptability and accuracy in practical application scenarios. By holistically considering the differential characteristics of spectral data and wavelength sensitivity, this research establishes a precise and pragmatic model optimization pathway, thereby enhancing the scientific integrity of the model while ensuring its effectiveness and reliability in addressing complex real-world application challenges.

In the context of monitoring salt damage in murals using hyperspectral data, dimensionality reduction serves as a primary method for identifying specific wavelengths. Principal Component Analysis (PCA) is employed to eliminate redundant information among variables and to extract as much useful information from the data as possible; it is also one of the more commonly used methods [27]. However, a major drawback of PCA in processing hyperspectral data is its reliance on linear assumptions, which may not effectively address the data's nonlinear characteristics and local structures, and the principal components generated are often difficult to interpret [65]. Given these limitations of PCA in handling hyperspectral data, this study adopts the Partial Least Squares Regression (PLSR) model. PLSR is capable of handling nonlinear relationships and can more effectively identify and utilize correlations among variables, thereby enhancing the model's interpretability and predictive accuracy [56, 66, 67]. The results indicate that the PTSR–PLSR model demonstrates a significant performance improvement over the previous PNDI–PLSR and PSR–PLSR models, specifically achieving a determination coefficient (Q^2) of 0.815 and reducing the Root Mean Square Error (RMSE) to 0.327, marking an accuracy improvement of 10.4% and 7.38%, respectively, compared to the PNDI–PLSR and PSR–PLSR models. These outcomes not only confirm the high accuracy and reliability of the PTSR–PLSR model in monitoring electrical conductivity in Mural Plaster but also highlight the potential application of FOD technology and refined spectral indices in the field of hyperspectral remote sensing monitoring.

To comprehensively assess its generalizability and ensure the unbiased nature of our findings, we conducted validation work on an independent testing set, a crucial step in understanding and confirming the efficacy of the three-band spectral index (Fig. 18). Although the prediction accuracy on this testing set was 0.716, lower than the 0.815 observed in the training set, the results still underscore the model's effectiveness and generalization capabilities in handling unseen data. This discrepancy in accuracy might point to challenges specific to the testing data, such as diversity and distribution differences, which are potential factors impacting generalizability. Furthermore, the use of an independent testing set enhances our understanding of the model's real-world performance and provides valuable data support for further optimization and application of the three-band spectral index, ensuring the objectivity and impartiality of our research outcomes. This not only demonstrates the practical value of the three-band spectral index but also offers guidance for future research directions.

Limitations of this study and future research directions

The limitations of this study are primarily reflected in the following aspects: First, although the efficacy of the PTSR three-band spectral index has been demonstrated to surpass that of the PNDI and PSR two-band spectral indices, an exhaustive horizontal comparison between different model construction forms (such as normalization, quadratic, logarithmic, exponential, etc.) and their relationship with specific study objects has not been conducted. This lack of comprehensive comparison limits a full understanding of the factors affecting model accuracy. Moreover, the potential application of machine learning methods to enhance computational efficiency has not been fully explored, which may hinder the efficiency improvement of hyperspectral data processing and analysis. Additionally, while the Partial Least Squares Regression (PLSR) model has been proven effective, insufficient exploration of its alternative methodologies restricts the possibilities for model optimization and innovation. Finally, the study's methods have not been further validated through field tests using hyperspectral cameras, limiting the understanding of the research method's field application effectiveness. Future research directions will focus on these limitations, especially on exploring the application effectiveness of hyperspectral cameras under complex field conditions through field testing; systematically comparing and analyzing different forms of three-band spectral index construction to identify the most suitable model types; and seeking effective alternatives to Partial Least Squares Regression to optimize existing models, enhancing their accuracy and practicality. These research directions will not only help overcome current limitations but will also advance the application and development of hyperspectral technology in soil component monitoring and other fields.

Conclusions

This study successfully developed an inversion model for estimating the Electrical Conductivity (EC) values of Mural Plaster subjected to phosphate erosion. The model leverages Fractional Order Differentiation (FOD) combined with a novel three-band spectral index and Partial Least Squares Regression algorithm.

Through qualitative experimental analysis of samples subjected to phosphate erosion, this study has discerned the emergence of irregularly shaped crystal clusters on the surfaces of these samples, displaying uneven characteristics. The occurrence of cracks, along with the delamination and morphological alterations of the material matrix, underscores that this experimental methodology more accurately approximates the actual conditions of salt damage suffered by murals. It enables an in-depth investigation into the specific mechanisms by which salinity affects murals at a microscopic level, offering a more precise and practical scientific foundation for the conservation of murals. Furthermore, this research explores the absorption mechanisms and characteristic spectral bands of the Electrical Conductivity (EC) values measured from Mural Plaster after phosphate erosion. By integrating the optimal spectral indices, a univariate linear regression model is constructed, providing a basis for rapid quantitative measurement of the mural's electrical conductivity. Notably, after applying a 0.3-order fractional order differentiation to the PSR and PNDI data, the model achieved optimal performance with an R^2 of 0.728, indicating that fractional order differentiation significantly enhances the model's predictive accuracy. Ultimately, employing the PLSR method and using a combination of the previously determined optimal six-order three-band spectral indices as explanatory variables, with EC values as the response variable, the fractional order differentiation combined with a novel three-band spectral index and Partial Least Squares Regression algorithm-based mural electrical conductivity high-spectral feature inversion model achieved an R^2 of 0.815. This further validates the model's efficiency and precision in monitoring salt damage in Dunhuang murals.

To summarize, this investigation not only furnishes an efficacious technological method for safeguarding esteemed cultural legacies such as the Dunhuang murals but also unveils the prospective applications of Fractional Order Differentiation (FOD) technology and three-band spectral indices within the sphere of hyperspectral remote sensing surveillance. It offers crucial insights and serves as a pertinent reference for subsequent inquiries in analogous fields.

Acknowledgements

The authors wish to express their sincere gratitude for the financial support received for this study. Our appreciation extends to the Municipal University Basic Research Business Fund Project (Grant No. X18092), which provided foundational support for our research endeavors. Additionally, we acknowledge the University Research Fund Natural Science Project-Doctoral Research Start-up Fund (Grant No. ZF15058) for facilitating the initial stages of our doctoral research work. The contributions of commercial research funds (Grant Nos. H23291 and H21133) have been instrumental in advancing our research to commercial application potentials. Moreover, our project has been significantly bolstered by the National Key R&D Program (Grant No. 2023YFC3803905), whose support has been pivotal in realizing the goals of this research. We are also grateful for the Science and Technology Project Support by STATE GRID Corporation of China (Grant No. 5200-202456108A-1-1-ZN), which has significantly contributed to the advancement of our work. Each of these funding bodies has played a crucial role in the progression and success of our study, and for that, we are profoundly thankful.

Author contributions

Conceptualization, Yikang Ren and Fang Liu; methodology, Yikang Ren; software, Yikang Ren; validation, Yikang Ren, Fang Liu; formal analysis, Yikang Ren; investigation, Yikang Ren; resources, Fang Liu; data curation, Fang Liu;

writing—original draft preparation, Yikang Ren; writing—review and editing, Fang Liu; visualization, Yikang Ren; supervision, Fang Liu; project administration, Yikang Ren; funding acquisition, Fang Liu. All authors have read and agreed to the published version of the manuscript.

Funding
The study was sponsored by Municipal University Basic Research Business Fund Project (X18092), University Research Fund Natural Science Project-Doctoral Research Start-up Fund (ZF15058), commercial research funds (H23291, H21133) National Key R&D Program (2023YFC3803905), Science and Technology Project Support by STATE GRID Corporation of China (5200-202456108A-1-1-ZN).

Availability of data and materials
No datasets were generated or analysed during the current study.

Declarations

Ethics approval and consent to participate
Not applicable.

Competing interests
The authors declare no competing interests.

Author details
[1]School of Geomatics and Urban Spatial Informatics, Beijing University of Civil Engineering and Architecture, Beijing 102616, China. [2]Key Laboratory of Urban Spatial Information, Ministry of Natural Resources, KLUSI, Beijing 100044, China.

Received: 8 June 2024 Accepted: 21 July 2024
Published online: 06 August 2024

References

1. Deng X, Yu Y. Ancient mural inpainting via structure information guided two-branch model. Herit Sci. 2023;11:131.
2. Xu Z, Zhang C, Wu Y. Digital inpainting of mural images based on DC-CycleGAN. Herit Sci. 2023;11:169.
3. Wang Z, Yin Y, Shan Z, Cui Q, Zhang W, Chai B, Li D, Yu Z, Su B. In-situ non-invasive analysis of conservation materials on mural paintings: a systematic approach in Dahuting Han Dynasty Tomb. Herit Sci. 2024;12:51.
4. Wright V, Meneses IA, Laval É. The origins of mural painting in Ancient Peru: archaeometric preliminary study of the Ventarrón mural paintings, valle de Lambayeque. Herit Sci. 2015;3:1–10.
5. Bolong C, Zongren Y, Manli S, Zhongwei S, Jinli Z, Biwen S, Zhuo W, Yaopeng Y, Bomin S. Virtual reconstruction of the painting process and original colors of a color-changed Northern Wei Dynasty mural in Cave 254 of the Mogao Grottoes. Herit Sci. 2022;10:164.
6. Scrivano S, Gaggero L. An experimental investigation into the salt-weathering susceptibility of building limestones. Rock Mech Rock Eng. 2020;53:5329–43.
7. Doehne E. Salt weathering: a selective review. Geol Soc Lond Special Publ. 2002;205:51–64.
8. Zhenyan S, Bingzhuo Y, Huyuan Z. Soluble salt distribution and environmental monitoring of Cave 276 in the Mogao Grottoes. J Lanzhou Univ Nat Sci. 2021;57:226–32.
9. Hongying D, Lei Z, Bomin S, Zhide H. Rapid detection and analysis the salt damage of Dunhuang Frescoes by Capillary Electrophoresis. Dunhuang Res. 2009;06:44–9, 123–4.
10. Zongren Y, Yanwu W, Xiaowei W. Research on the water vapor source induced diseases of wall paintings in Longxing Temple. Adv Earth Sci. 2017;32:668–76.
11. Ma J, Zheng B, He Y. Applications of a hyperspectral imaging system used to estimate wheat grain protein: a review. Front Plant Sci. 2022;13:837200.
12. Patel AK, Ghosh JK, Pande S, Sayyad SU. Deep-learning-based approach for estimation of fractional abundance of nitrogen in soil from hyperspectral data. IEEE J Sel Top Appl Earth Obs Remote Sens. 2020;13:6495–511.
13. Katsumi S, Saigusa M, Ito F. Molecular aggregation dynamics via a liquid-like cluster intermediate during heterogeneous evaporation as revealed by hyperspectral camera fluorescence imaging. J Phys Chem B. 2022;126:976–84.
14. Yan Y, Ren J, Zhao H, Windmill JF, Ijomah W, De Wit J, Von Freeden J. Non-destructive testing of composite fiber materials with hyperspectral imaging—evaluative studies in the EU H2020 FibreEUse project. IEEE Trans Instrum Meas. 2022;71:1–13.
15. Gong Y, Li X, Lv L, Zhang B, Xuan J, Du H. Using UAV LiDAR intensity frequency and hyperspectral features to improve the accuracy of urban tree species classification. IEEE J Sel Top Appl Earth Obs Remote Sens. 2023.
16. Liu Y, Lyu S, Hou M, Gao Z, Wang W, Zhou X. A novel spectral matching approach for pigment: spectral subsection identification considering ion absorption characteristics. Remote Sens. 2020;12:3415.
17. Zhouqian G, Shuqiang L, Miaole H. Inversion of salt content in simulated mural based on hyperspectral mural salt index. Spectrosc Spectr Anal. 2023;43:3272–9.
18. Sansupa C, Suphaphimol N, Nonthijun P, Ronsuek T, Yimklan S, Semakul N, Khrueraya T, Suwannarach N, Purahong W, Disayathanoowat T. Life on the wall: the diversity and activity of microbes on 13th-century AD. Lan Na mural painting. Front Microbiol. 2023;14:1220901.
19. Sharma A, Singh MR, Jangid R. Scientific study of the pigments and binders used in mural painting from the 16th-century ce St Mary's Church of Cheriapally, Kottyam, Kerala, and its relevance to conservation. Archaeometry. 2023;65:617–34.
20. Małysiak A, Orda S, Drzazga M. Influence of supersaturation, temperature and rotational speed on induction time of calcium sulfate crystallization. Crystals. 2021;11:1236.
21. Rizwan M, Gilani SR, Durani AI, Naseem S. Materials diversity of hydrogel: synthesis, polymerization process and soil conditioning properties in agricultural field. J Adv Res. 2021;33:15–40.
22. Mashimbye Z, Cho M, Nell J, De Clercq W, Van Niekerk A, Turner D. Model-based integrated methods for quantitative estimation of soil salinity from hyperspectral remote sensing data: a case study of selected South African soils. Pedosphere. 2012;22:640–9.
23. Xu C, Zeng W, Huang J, Wu J, Van Leeuwen WJ. Prediction of soil moisture content and soil salt concentration from hyperspectral laboratory and field data. Remote Sens. 2016;8:42.
24. Hu J, Peng J, Zhou Y, Xu D, Zhao R, Jiang Q, Fu T, Wang F, Shi Z. Quantitative estimation of soil salinity using UAV-borne hyperspectral and satellite multispectral images. Remote Sens. 2019;11:736.
25. Zhong Q, Eziz M, Sawut R, Ainiwaer M, Li H, Wang L. Application of a hyperspectral remote sensing model for the inversion of nickel content in urban soil. Sustainability. 2023;15:13948.
26. Hou Y, Zhang F. Estimation model of desert soil organic matter content using hyperspectral data. Trans Chin Soc Agric Eng. 2014;30:113–20.
27. Zhang J, Jing X, Song X, Zhang T, Duan W, Su J. Hyperspectral estimation of wheat stripe rust using fractional order differential equations and Gaussian process methods. Comput Electron Agric. 2023;206: 107671.
28. Liu Y, Lu Y, Chen D, Zheng W, Ma Y, Pan X. Simultaneous estimation of multiple soil properties under moist conditions using fractional-order derivative of vis-NIR spectra and deep learning. Geoderma. 2023;438:116653.
29. Zhang Z, Ding J, Wang J, Ge X. Prediction of soil organic matter in northwestern China using fractional-order derivative spectroscopy and modified normalized difference indices. CATENA. 2020;185: 104257.
30. Ge X, Ding J, Teng D, Xie B, Zhang X, Wang J, Han L, Bao Q, Wang J. Exploring the capability of Gaofen-5 hyperspectral data for assessing soil salinity risks. Int J Appl Earth Obs Geoinf. 2022;112: 102969.
31. Noda I. Progress in two-dimensional (2D) correlation spectroscopy. J Mol Struct. 2006;799:2–15.
32. Chen L, Lai J, Tan K, Wang X, Chen Y, Ding J. Development of a soil heavy metal estimation method based on a spectral index: combining fractional-order derivative pretreatment and the absorption mechanism. Sci Total Environ. 2022;813: 151882.
33. Yuan J, Gao J, Yu B, Yan C, Ma C, Xu J, Liu Y. Estimation of soil organic matter content based on spectral indices constructed by improved Hapke model. Geoderma. 2024;443: 116823.
34. Jia P, Zhang J, He W, Hu Y, Zeng R, Zamanian K, Jia K, Zhao X. Combination of hyperspectral and machine learning to invert soil electrical conductivity. Remote Sens. 2022;14:2602.

35. Dong T, Wu B. Estimate faction of photosynthetically active radiation with three-band vegetation indices based on HJ-CDD satellite in wheat. In: 2012 first international conference on agro-geoinformatics (agro-geoinformatics), IEEE. 2012. p. 1–5.
36. Gangquan, C. Study on salting damage analysis and treatment of wall paintings at Mogao Grottoes, Dunhuang. 博士, 2016.
37. Bi W. Study on coupled heat and mass transfer process and characteristics of earthen plasters in Mogao Grottoes. Doctor, Xi'an University of Architecture and Technology; 2022.
38. Ayanleye S, Nasir V, Avramidis S, Cool J. Effect of wood surface roughness on prediction of structural timber properties by infrared spectroscopy using ANFIS, ANN and PLS regression. Eur J Wood Wood Prod. 2021;79:101–15.
39. Zhang X, Huang B. Prediction of soil salinity with soil-reflected spectra: a comparison of two regression methods. Sci Rep. 2019;9:5067.
40. Chen J, Jönsson P, Tamura M, Gu Z, Matsushita B, Eklundh L. A simple method for reconstructing a high-quality NDVI time-series data set based on the Savitzky-Golay filter. Remote Sens Environ. 2004;91:332–44.
41. Petráš I, Magin RL. Simulation of drug uptake in a two compartmental fractional model for a biological system. Commun Nonlinear Sci Numer Simul. 2011;16:4588–95.
42. Wang X, Zhang F, Kung H-T, Johnson VC, Latif A. Extracting soil salinization information with a fractional-order filtering algorithm and grid-search support vector machine (GS-SVM) model. Int J Remote Sens. 2020;41:953–73.
43. Kahaer Y, Tashpolat N. Estimating salt concentrations based on optimized spectral indices in soils with regional heterogeneity. J Spectrosc. 2019;2019:2402749.
44. Lv S, Wang J, Wang S, Wang Q, Wang Z, Fang Y, Zhai W, Wang F, Qu G, Ma W. Quantitative analysis of chlorophyll in *Catalpa bungei* leaves based on partial least squares regression and spectral reflectance index. Sci Hortic. 2024;329: 113019.
45. Cao Z, Wang Q, Zheng C. Best hyperspectral indices for tracing leaf water status as determined from leaf dehydration experiments. Ecol Indic. 2015;54:96–107.
46. Lee Rodgers J, Nicewander WA. Thirteen ways to look at the correlation coefficient. Am Stat. 1988;42:59–66.
47. Chen X, Li F, Shi B, Fan K, Li Z, Chang Q. Estimation of winter wheat canopy chlorophyll content based on canopy spectral transformation and machine learning method. Agronomy. 2023;13:783.
48. Peng S, Bao N, Wang S, Gholizadeh A, Saberioon M, Peng Y. Mapping vertical distribution of SOC and TN in reclaimed mine soils using point and imaging spectroscopy. Ecol Ind. 2024;158: 111437.
49. Tian A, Zhao J, Tang B, Zhu D, Fu C, Xiong H. Hyperspectral prediction of soil total salt content by different disturbance degree under a fractional-order differential model with differing spectral transformations. Remote Sens. 2021;13:4283.
50. Zhang F, Tiyip T, Ding J, Kung H, Johnson VC, Sawut M, Tashpolat N, Gui D. Studies on the reflectance spectral features of saline soil along the middle reaches of Tarim River: a case study in Xinjiang Autonomous Region, China. Environ Earth Sci. 2013;69:2743–61.
51. Wang Q, Li P, Chen X. Modeling salinity effects on soil reflectance under various moisture conditions and its inverse application: a laboratory experiment. Geoderma. 2012;170:103–11.
52. Madejová J. FTIR techniques in clay mineral studies. Vib Spectrosc. 2003;31:1–10.
53. Horneck DA, Ellsworth JW, Hopkins BG, Sullivan DM, Stevens RG. Managing salt-affected soils for crop production. 2007.
54. Goj P, Handke B, Stoch P. Vibrational characteristics of aluminum–phosphate compounds by an experimental and theoretical approach. Sci Rep. 2022;12:17495.
55. Weidong L, Baret F, Xingfa G, Qingxi T, Lanfen Z, Bing Z. Relating soil surface moisture to reflectance. Remote Sens Environ. 2002;81:238–46.
56. Song G, Wang Q, Jin J. Fractional-order derivative spectral transformations improved partial least squares regression estimation of photosynthetic capacity from hyperspectral reflectance. IEEE Trans Geosci Remote Sens. 2023;61:1–10.
57. Jin H, Peng J, Bi R, Tian H, Zhu H, Ding H. Comparing laboratory and satellite hyperspectral predictions of soil organic carbon in farmland. Agronomy. 2024;14:175.
58. Zhang A, Yin S, Wang J, He N, Chai S, Pang H. Grassland chlorophyll content estimation from drone hyperspectral images combined with fractional-order derivative. Remote Sens. 2023;15:5623.
59. Hong Y, Liu Y, Chen Y, Liu Y, Yu L, Liu Y, Cheng H. Application of fractional-order derivative in the quantitative estimation of soil organic matter content through visible and near-infrared spectroscopy. Geoderma. 2019;337:758–69.
60. Xu X, Chen S, Xu Z, Yu Y, Zhang S, Dai R. Exploring appropriate preprocessing techniques for hyperspectral soil organic matter content estimation in black soil area. Remote Sens. 2020;12:3765.
61. Mishra P, Biancolillo A, Roger JM, Marini F, Rutledge DN. New data preprocessing trends based on ensemble of multiple preprocessing techniques. TrAC Trends Anal Chem. 2020;132: 116045.
62. Fu C-B, Xiong H-G, Tian A-H. Study on the effect of fractional derivative on the hyperspectral data of soil organic matter content in arid region. J Spectrosc. 2019;2019:7159317.
63. Wang X, Zhang F, Ding J, Latif A, Johnson VC. Estimation of soil salt content (SSC) in the Ebinur Lake Wetland National Nature Reserve (ELWNNR), Northwest China, based on a Bootstrap-BP neural network model and optimal spectral indices. Sci Total Environ. 2018;615:918–30.
64. Zhou X, Zhang F, Liu C, Kung H-T, Johnson VC. Soil salinity inversion based on novel spectral index. Environ Earth Sci. 2021;80:501.
65. Wang B, Sun J, Xia L, Liu J, Wang Z, Li P, Guo Y, Sun X. The applications of hyperspectral imaging technology for agricultural products quality analysis: a review. Food Rev Intl. 2023;39:1043–62.
66. Song G, Wang Q, Jin J. Temporal instability of partial least squares regressions for estimating leaf photosynthetic traits from hyperspectral information. J Plant Physiol. 2022;279: 153831.
67. Jin J, Wu M, Song G, Wang Q. Genetic algorithm captured the informative bands for partial least squares regression better on retrieving leaf nitrogen from hyperspectral reflectance. Remote Sens. 2022;14:5204.

Publisher's Note